

₁ Study of neutrino-nucleus interaction at around 1 GeV using
₂ a 3D grid-structure neutrino detector, WAGASCI, muon
₃ range detectors and magnetized spectrometer, Baby MIND,
₄ at J-PARC neutrino monitor hall

₅ A. Bonnemaison, R. Cornat, L. Domine, O. Drapier, O. Ferreira, F. Gastaldi,
₆ M. Gonin, J. Imber, M. Licciardi, F. Magniette, T. Mueller, L. Vignoli, and O. Volcy
₇ *Ecole Polytechnique, IN2P3-CNRS, Laboratoire Leprince-Ringuet, Palaiseau,*
₈ *France*

₉ S. Cao and T. Kobayashi

₁₀ *High Energy Accelerator Research Organization (KEK), Tsukuba, Ibaraki, Japan*

₁₁ M. Khabibullin, A. Khotjantsev, A. Kostin, Y. Kudenko, A. Mefodiev, O. Mineev,
₁₂ S. Suvorov, and N. Yershov

₁₃ *Institute for Nuclear Research of the Russian Academy of Sciences, Moscow, Russia*

₁₄ B. Quilain

₁₅ *Kavli Institute for the Physics and Mathematics of the Universe (WPI), The*
₁₆ *University of Tokyo Institutes for Advanced Study, University of Tokyo, Kashiwa,*
₁₇ *Chiba, Japan*

₁₈ T. Hayashino, A. Hiramoto, A.K. Ichikawa, K. Nakamura, T. Nakaya, K Yasutome,
₁₉ and K. Yoshida

₂₀ *Kyoto University, Department of Physics, Kyoto, Japan*

₂₁ Y. Azuma, J. Harada, T. Inoue, K. Kin, N. Kukita, S. Tanaka, Y. Seiya,
₂₂ K. Wakamatsu, and K. Yamamoto

₂₃ *Osaka City University, Department of Physics, Osaka, Japan*

24 A. Blondel, F. Cadoux, Y. Favere, E. Noah, L. Nicola, and S. Parsa

25 *University of Geneva, Section de Physique, DPNC, Geneva, Switzerland*

26 N. Chikuma, F. Hosomi, T. Koga, R. Tamura, and M. Yokoyama

27 *University of Tokyo, Department of Physics, Tokyo, Japan*

28 Y. Hayato

29 *University of Tokyo, Institute for Cosmic Ray Research, Kamioka Observatory,*
30 *Kamioka, Japan*

31 Y. Asada, K. Matsushita, A. Minamino, K. Okamoto, and D. Yamaguchi

32 *Yokohama National University, Faculty of Engineering, Yokohama, Japan*

33 December 14, 2017

34 **Contents**

35	1	Introduction	3
36	2	Experimental Setup	4
37	2.1	Wagasci modules	5
38	2.1.1	Detector	5
39	2.1.2	Electronics	8
40	2.1.3	Water system	9
41	2.2	INGRID Proton module	10
42	2.3	Baby MIND	11
43	2.3.1	Magnet modules	11
44	2.3.2	Scintillator modules	12
45	2.3.3	Electronics	14
46	2.3.4	Pefromance check	15
47	2.4	Side muon range detector	16

48	3 Physics goals	18
49	3.1 Expected number of events	19
50	3.2 Pseudo-monochromatic beam by using different off-axis fluxes	19
51	3.3 Subjects Wagasci can contribute	20
52	4 Status of J-PARC T59 experiment	22
53	5 MC studies	26
54	5.1 Detector simulation	26
55	5.1.1 Detector geometry	26
56	5.1.2 Response of detector components	26
57	5.2 Track reconstruction	26
58	5.3 Event selection	27
59	5.4 Cross section measurements	29
60	6 Standalone WAGASCI-module performances	30
61	6.1 Reconstruction algorithm	32
62	6.1.1 Description	32
63	6.1.2 Performances	34
64	6.2 Background subtraction: the water-out module	38
65	7 Schedule	41
66	8 Requests	41
67	8.1 Neutrino beam	41
68	8.2 Equipment request including power line	41

69 **1 Introduction**

70 The understanding of neutrino-nucleus interactions in the 1 GeV energy region is critical
 71 for the success of accelerator-based neutrino oscillation experiments such as the T2K exper-
 72 iment. Complicated multi-body effects of nuclei render this understanding difficult. The
 73 T2K near detectors have been measuring these and significant progress has been achieved.
 74 However, the understanding is still limited. One of the big factors preventing from full
 75 understanding is the non-monochromatic neutrino beam spectrum. Measurements with
 76 different but some overlapping beam spectra would greatly benefit to resolve the contrib-
 77 ution from different neutrino energies. We, the Wagasci collaboration, proposes to study
 78 the neutrino-nucleus interaction at the B2 floor of the neutrino monitor building, where
 79 different neutrino spectra can be obtained due to the different off-axis position. Our exper-
 80 imental setup contains 3D grid-structure plastic-scintillator detectors filled with water as
 81 the neutrino interaction target (Wagasci modules), two side- and one downstream- muon

range detectors(MRD's). The 3D grid-structure and side-MRD's allows a measurement of wider-angle scattering than the T2K off-axis near detector (ND280). High water to scintillator material ratio enables the measurement of the neutrino interaction on water, which is highly desired for the T2K experiment because it's far detector, Super-Kamiokande, is composed of water. The MRD's consist of plastic scintillators and iron plates. The downstream-MRD, so called the Baby MIND detector, also works as a magnet and provides the charge identification capability as well as magnetic momentum measurement for high energy muons. The charge identification is essentially important to select antineutrino events in the antineutrino beam because contamination of the neutrino events is as high as 30%. Most of the detectors has been already constructed. The Wagasci modules have been commissioned as the J-PARC T59 experiment and the Baby MIND detector was commissioned at the CERN neutrino platform. Therefore, the collaboration will be ready to proceed to the physics data taking for the T2K beam time in January 2019. We will provide the cross sections of the charged current neutrino and antineutrino interactions on water with slightly higher neutrino energy than T2K ND280 with wide angler acceptance. When combined with ND280 measurements, our measurement would greatly improve the understanding of the neutrino interaction at around 1 GeV and contribute to reduce one of the most significant uncertainty of the T2K experiment.

2 Experimental Setup

Figure. 1 and 2 show a schematic view and a CAD drawing of the entire set of detectors. Central neutrino target detectors consist of two Wagasci modules and T2K INGRID proton module. Inside the Wagasci module, plastic scintillator bars are aligned as a 3D grid-like structure and spaces in the structure are filled with water for a water-in Wagasci module. T2K INGRID proton module is a full active neutrino target detector which is composed only with scintillator bars in its tracking region. The central detectors are surrounded by two side- and one downstream- muon range detectors(MRD's) The MRD's are used to select muon tracks from the charged-current (CC) interactions and to reject short tracks caused by neutral particles that originate mainly from neutrino interactions in material surrounding the central detector, like the walls of the detector hall, neutrons and gammas, or neutral-current (NC) interactions. The muon momentum can be reconstructed from its range inside the detector. The MRD's consist of plastic scintillators and iron plates. In addition, each of the iron plates of the downstream-MRD, so called the Baby MIND detector, is wound by a coil and can be magnetized. It provide the charge selection capability.

For all detectors, scintillation light in the scintillator bar is collected and transported to a photodetector with a wavelength shifting fiber (WLS fiber). The light is read out by a photodetector, Multi-Pixel Photon Counter (MPPC), attached to one end of the WLS fiber. The signal from the MPPC is read out by the dedicated electronics developed for the test experiment to enable bunch separation in the beam spill. The readout electronics is

120 triggered using the beam-timing signal from MR to synchronize to the beam. The beam-
121 timing signal is branched from those for T2K, and will not cause any effect on the T2K
122 data taking.

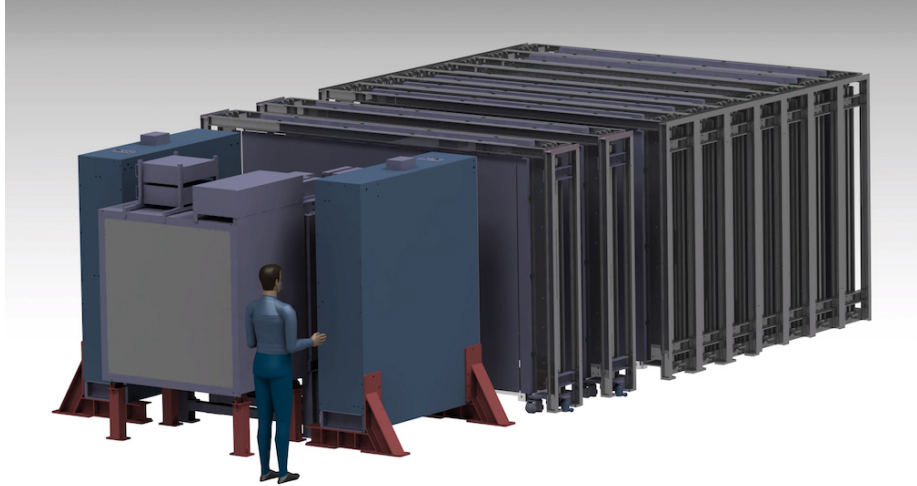


Figure 1: Schematic view of entire sets of detectors.

123 T2K adopted the off-axis beam method, in which the neutrino beam is intentionally
124 directed 2.5 degrees away from SK producing a narrow band ν_μ beam. The off-axis near
125 detector, ND280, is installed towards the SK direction in the B1 floor of the near detector
126 hall of the J-PARC neutrino beam-line. We propose to install our detector in the B2 floor
127 of the near detector hall, where the off-axis angle is similar but slightly different: 1.5 degree.
128 The candidate detector position in the B2 floor is shown in Fig. 3. The expected neutrino
129 energy spectrum at the candidate position is shown in Fig. 4.

130 2.1 Wagasci modules

131 2.1.1 Detector

132 The WAGASCI modules are mainly composed of 1280 plastic scintillator bars and a sur-
133 rounding stainless steel tank as shown in Fig. 5. The total number of channels in one
134 Wagasci module is 1280. The stainless steel tank is constructed by welding stainless steel
135 plates, is sized as $46 \times 125 \times 125 \text{ cm}^3$, and weighs 0.5 ton.

136 One Wagasci module consists of 16 scintillator tracking planes, where each plane is an
137 array of 80 scintillator bars fixed with ABS frames. The 40 bars, called parallel scintillators,
138 are placed perpendicularly to the beam, and the other 40 bars, called grid scintillators, are
139 placed in parallel to the beam with grid structure in the tracking plane as shown in Fig.

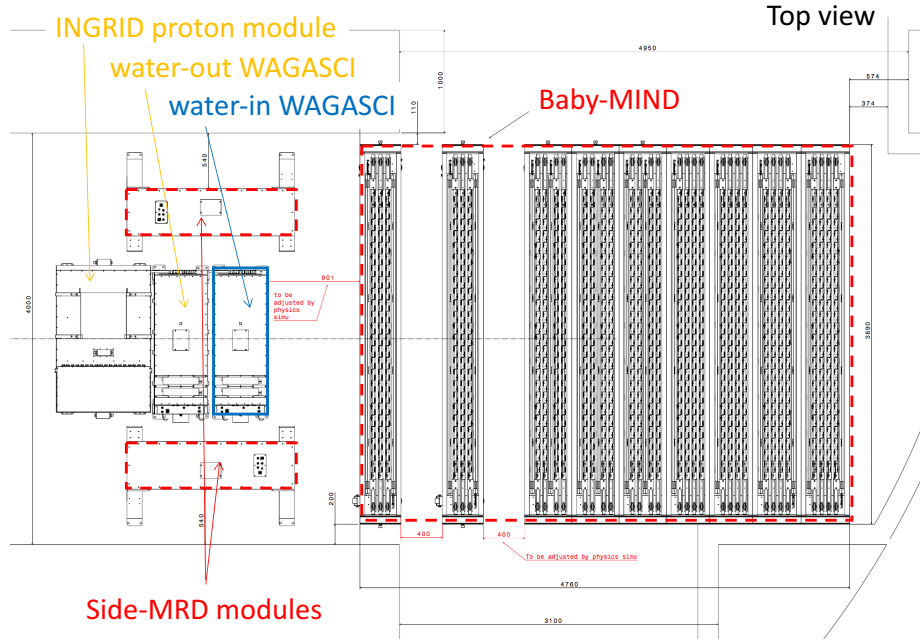


Figure 2: Top view of entire sets of detectors.

140 5. Thanks to the 3 D grid-like structure of the scintillator bars, the Wagasci module has
 141 4π angular acceptance for charged particles.

142 Thin plastic scintillator bars produced at Fermilab by extrusion method, mainly consists
 143 of polystyrene and are surrounded by thin reflector including TiO_2 (3 mm in thickness)
 144 are used for the Wagasci modules to reduce the mass ratio of scintillator bars to water,
 145 because neutrino interactions in the scintillator bars are a background for the cross section
 146 measurements on H_2O . Each scintillator bar is sized as $1020 \times 25 \times 3 \text{ mm}^3$ including the
 147 reflector part, and half of all the scintillator bars have 5-cm-interval slits to form the grid
 148 structure (Figure 6).

149 We will have two types of the Wagasci modules, a water-in module and a water-out
 150 module. The water-in Wagasci module has water in spaces of the grid structure. The total
 151 water mass serving as neutrino targets in the fiducial volume of the module is 188 kg, and
 152 the mass ratio of scintillator bars to water is 80 %. The water-out Wagasci module doesn't
 153 have water inside the detector. The total CH mass serving as neutrino target in the fiducial
 154 volume of the module is 47 kg, and the mass fraction of scintillator bars is 100 %.

155 Scintillation light is collected by wave length shifting fibers, Y-11 (non-S type with a
 156 diameter of 1.0 mm produced by Kuraray. A fiber is glued by optical cement in a groove
 157 on surface of a scintillator bar. 32 fibers are gathered together by a fiber bundle at edge

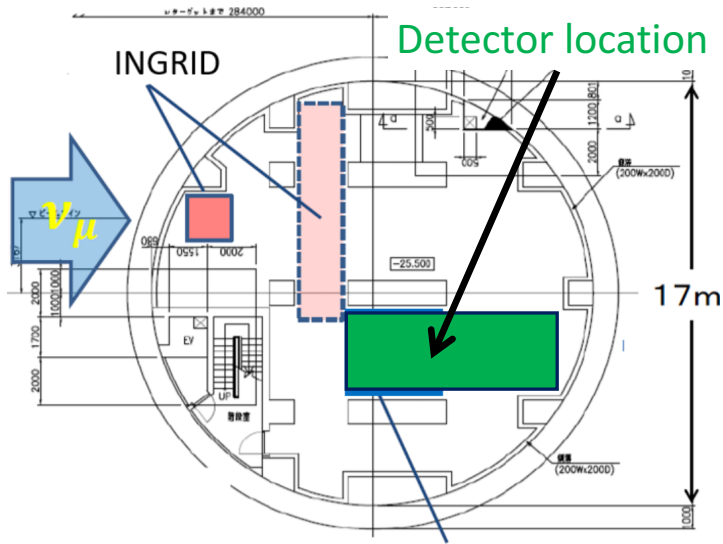


Figure 3: Candidate detector position in the B2 floor of the near detector hall.

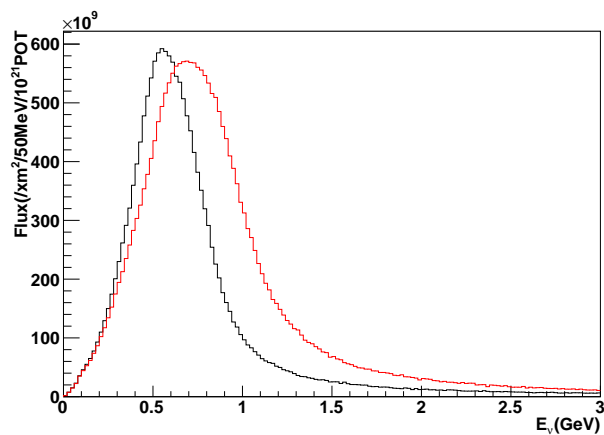


Figure 4: Neutrino energy spectrum at the candidate detector position (red, off-axis 1.5 degree). The spectrum at the ND280 site (black, off-axis 2.5 degree) is also shown.

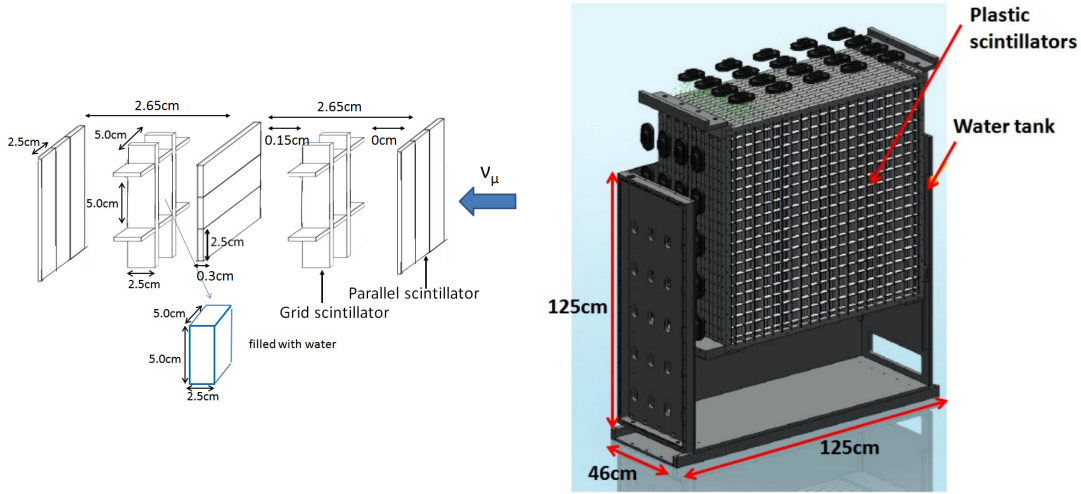


Figure 5: Schematic views of 3D grid-like structure of plastic scintillator bars (left) and Wagasci module (right).

158 of the module, and lead scintillation light to a 32-channel arrayed MPPC. Since crosstalk
 159 of light yield due to reflection on the inner surface of each cell has been observed, all the
 160 scintillator bars are painted black by aqueous color spray. It is confirmed by measurements
 161 with cosmic rays that black painting on the surface of the scintillator bars suppresses this
 162 crosstalk so that no significant crosstalk effect is observed within uncertainty.

163 32-channel arrayed MPPCs, as shown in the Fig. 7, are used for the modules. The
 164 surface of the fiber bundle is polished and directly attached onto the 32-channel arrayed
 165 MPPCs. The positions of 32 fibers on the bundle are aligned to fit the channels of MPPCs.
 166 The MPPC is a product of Hamamatsu Photonics, S13660(ES1), with suppressed noise
 167 rate of ~ 6 kHz per channel at 0.5 p.e. threshold. For each MPPC channel, 716 pixels of
 168 APD are aligned in a shape of circle.

169 2.1.2 Electronics

170 As front-end electronics of this detector, a Silicon PM Integrated Read-Out Chip (SPIROC)
 171 [12] is adopted. SPIROC is a 36-channel auto-triggered front-end ASIC, and is produced
 172 by OMEGA/ IN2P3. It not only contains an analog signal processing part such as amplification
 173 and shaping of the waveform, but contains a digital signal processing parts such as
 174 auto-trigger and timing measurement. Charge of MPPC signal is sampled by track-and-
 175 hold circuit. A Front-end electronics board, Active Sensor Unit (ASU), has been developed
 176 with the SPIROC2D chip, which is the latest version of SPIROC. Each readout board is
 177 designed to control a 32-channel arrayed MPPC, and 40 of the ASU boards are aligned on

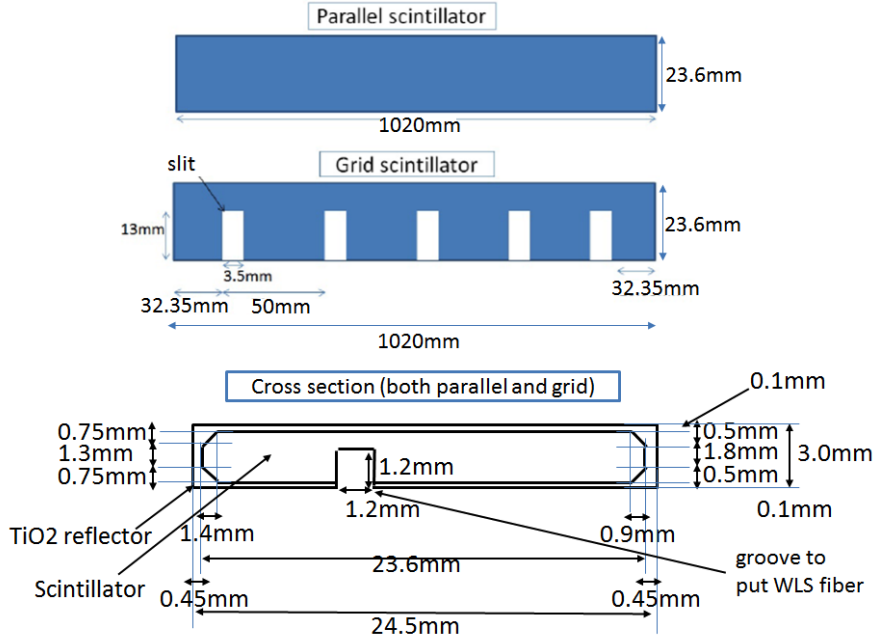


Figure 6: Geometry of scintillators used for Wagasci modules.

178 the module surface. The data acquisition system used for this detector, including back-end
 179 boards, has been developed for prototypes of ultra-granular calorimeters for the Interna-
 180 tional Linear Collider (ILC) [5], and independent of the T2K DAQ system. To synchronize
 181 the DAQ system to J- PARC neutrino beam, pre-beam trigger and beam trigger are sent to
 182 the clock control card. The beam trigger signals are converted from optical signals to NIM
 183 signals at NIM module on the B2 floor. In addition, the information of spill number are
 184 delivered with 16-bit ECL level signals, and converted to an Ethernet frame by an FPGA
 185 evaluation board to be directly sent to the DAQ PC. The electronics readout scheme is
 186 shown in Fig. 8.

187 **2.1.3 Water system**

188 Pure water is filled to the water tank of the water-in Wagasci module as follows. First,
 189 the water storage tank located at the B2 floor of the NM pit is filled with water delivered
 190 from a water tap on the ground level through a long hose. Second, the water is pumped
 191 to the other water storage tank though a water filler to produce pure water. Third, a
 192 compound preservative called Germall plus, which is the same preservative used in one of
 193 the sub-detectors of T2K ND280, FGD2, is put into the water to keep water from being
 194 bad. Then, the water is poured to the water-in Wagasci module, and it is kept in the

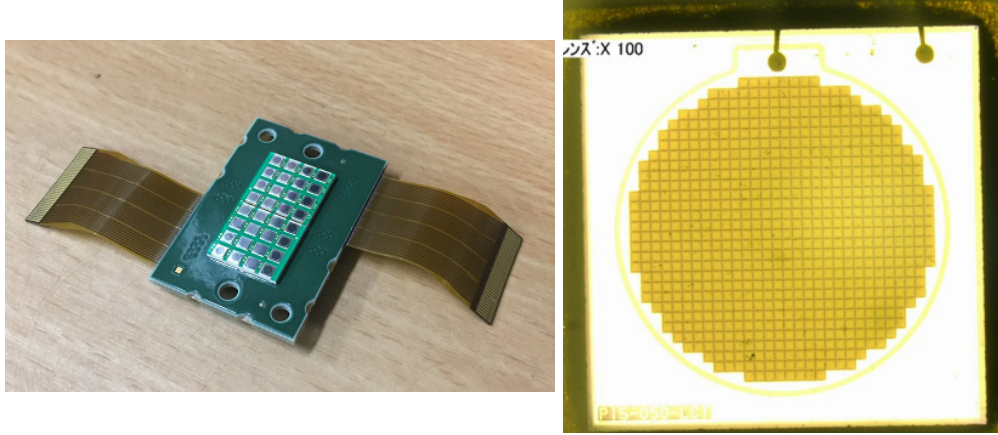


Figure 7: 32-channel arrayed MPPC (left) and an enlarged view of one MPPC channel (right).

195 module during the neutrino beam operation and not to be circulated.

196 2.2 INGRID Proton module

197 INGRID Proton module is a neutrino detectors of the T2K experiment. It is a fully-active
198 tracking detector which consists of only scintillator strips. The purpose of this Proton
199 Module is to separate the neutrino interaction types by detecting the protons and pions
200 together with the muons from the neutrino interactions, and to measure the neutrino cross
201 section for each interaction type. It consists of 36 tracking planes surrounded by veto planes
202 (Figure 9), where each tracking plane is an array of two types of scintillator strips. The
203 16 strips in the inner region have dimensions of $2.5\text{cm} \times 1.3\text{cm} \times 120\text{cm}$, while the 16 strips
204 in the outer region have dimensions of $5\text{cm} \times 1\text{cm} \times 120\text{cm}$, making a plane of $120 \times 120\text{cm}^2$
205 in the horizontal and vertical directions. The former is the scintillator produced for the
206 K2K SciBar detector [3] and the latter was produced for INGRID. The tracking planes are
207 placed perpendicular to the beam axis at 23mm intervals. Since the strips are aligned in one
208 direction, each tracking plane is sensitive to either the horizontal or vertical position of the
209 tracks. The tracking planes are therefore placed alternating in the horizontal and vertical
210 directions so that three-dimensional tracks can be reconstructed. The tracking planes also
211 serve as the neutrino interaction target. As with the Wagasci modules, scintillation light
212 is read out by a WLS fiber and MPPC.

213 It was installed at the neutrino beam axis on the SS floor of the T2K near detector hall
214 in 2010, and had been used for neutrino cross section measurements. In August 2017, it
215 was moved to the B2 floor of the T2K near detector hall by J-PARC T59 after getting the
216 approval from T2K to use them. J-PARC T59 is performing a neutrino beam measurement

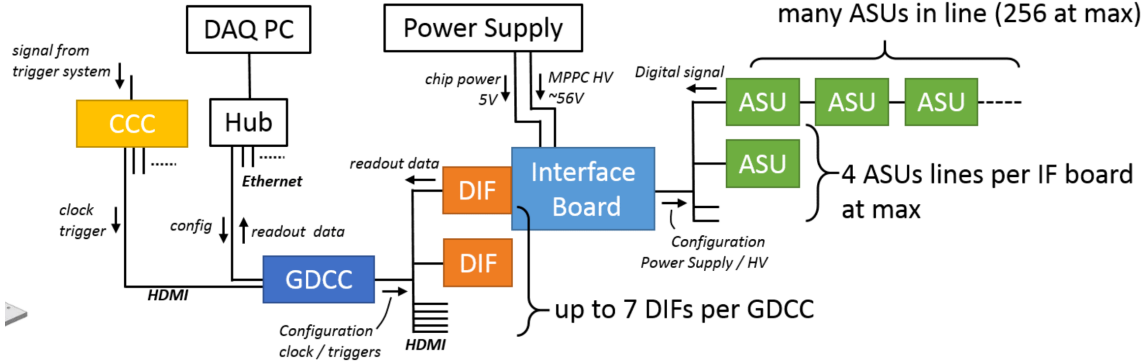


Figure 8: Wagasci electronics readout scheme.

217 using the detector from October 2017, and the measurement will continue until May 2018
 218 as we will discuss in Sec. 4.

219 We will operate the INGRID Proton module using the T2K near detector electronics/
 220 DAQ system in the same way as J-PARC T59. A proposal to use the module and its
 221 electronics for our project will be submitted to the T2K collaboration.

222 2.3 Baby MIND

223 The Baby MIND is the downstream Muon Range Detector. It also works as a magnet and
 224 provides the charge identification capability as well as magnetic momentum measurement
 225 for high energy muons.

226 The Baby MIND collaboration ¹ submitted a proposal to the SPSC at CERN, SPSC-P-
 227 353. The project was approved by the CERN research board as Neutrino Platform project
 228 NP05 and constructed. The detector consists of 33 magnet modules, each 3500 mm ×
 229 2000 mm × 50 mm (30 mm steel) with a mass of approximately 2 tonnes. Of these magnet
 230 modules, 18 are instrumented with plastic scintillator modules.

231 2.3.1 Magnet modules

232 The Baby MIND is built from sheets of iron interleaved with scintillator detector modules
 233 but unlike traditional layouts for magnetized iron neutrino detectors (e.g. MINOS) which
 234 tend to be monolithic blocks with a unique pitch between consecutive steel segments and
 235 large conductor coils threaded around the whole magnet volume, the Baby MIND iron
 236 segments are all individually magnetized as shown in Fig. 10, allowing for far greater
 237 flexibility in the setting of the pitch between segments, and in the allowable geometries
 238 that these detectors can take.

¹Contact person: E. Noah, Spokesperson: A. Blondel, Deputy spokesperson: Y. Kudenko

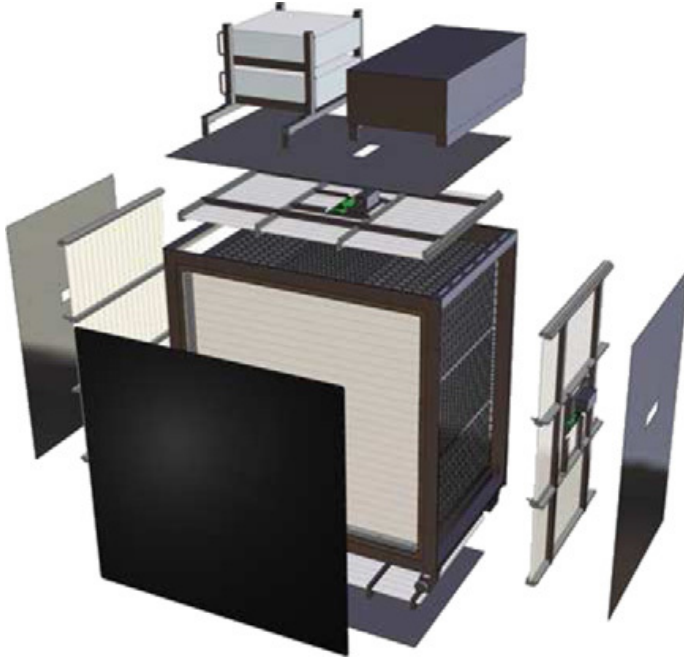


Figure 9: Schematic view of INGRID Proton module.

239 The key design outcome is a highly optimized magnetic field map. A double-slit con-
 240 figuration for coil winding was adopted to increase the area over which the magnetic flux
 241 lines are homogeneous in B_x across the central tracking region. Simulations show the
 242 magnet field map to be very uniform over this central tracking region covering an area of
 243 $2800 \times 2000 \text{ mm}^2$, Fig. 11. The B_x component dominates in this region, with negligible
 244 B_y and B_z . This was confirmed by measuring the field with 9 pick-up coils wound around
 245 the first module. Subsequent modules were equipped with one pick-up coil. Test results
 246 on the 33 modules show all to achieve the required field of 1.5 T for a current of 140 A,
 247 with a total power consumption of 11.5 kW. The polarity of the field map shown in Fig. 11
 248 (middle) can be reversed by changing the power supply configuration.

249 **2.3.2 Scintillator modules**

250 Each of the 18 scintillator modules is constructed from 2 planes of horizontal counters (95
 251 counters in total) and 2 planes of vertical counters (16 counters in total) [2], arranged
 252 with an overlap between planes to achieve close to 100% hit efficiency for minimum ioniz-
 253 ing muons. The arrangement of planes within a module is vertical-horizontal-horizontal-
 254 vertical. This arrangement was the result of an assembly approach whereby each plane
 255 was built from 2 half-planes, with each half plane consisting of a horizontal plane and a

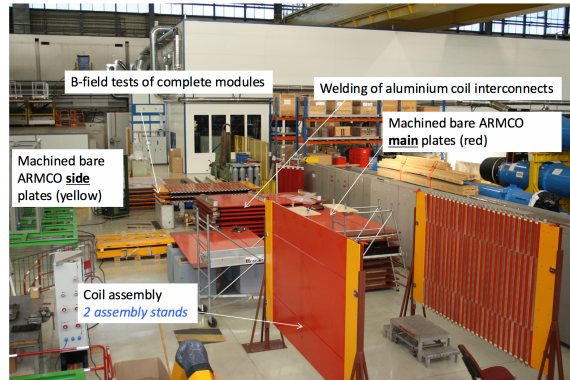


Figure 10: Magnet assembly zone at CERN.

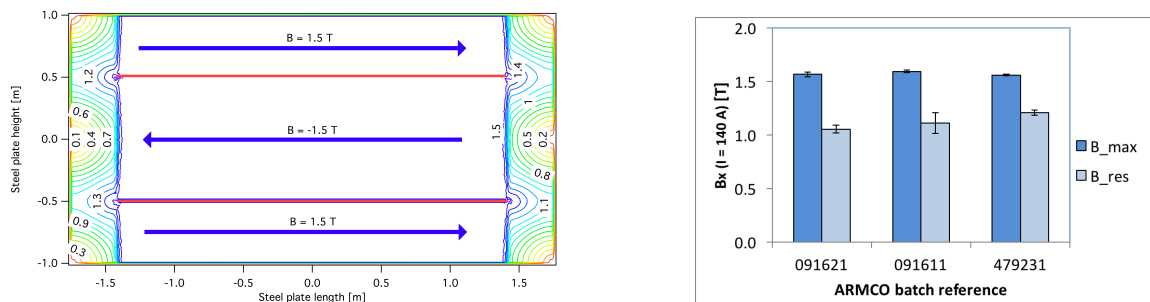


Figure 11: Left) Magnetic field map with a coil along 280 cm of the length of the plate. Right) Measured B field for 33 modules.

256 vertical plane. The scintillator bars are held in place using structural ladders that align
257 and maintain the counters, Fig. 12. No glue is used in the process, so counters can be
258 replaced. Aluminum sheets front and back provide light tightness.



Figure 12: Scintillator modules assembly. Left) top of front half-module showing vertical counters, and the spacers-ladders that set the pitch between horizontal counters and hold them in place. Middle) rear half-module showing horizontal counters on their ladders. Right) Assembled rear half-module, the front half-module can be seen in the background.

259 The plastic scintillator counters were made from 220 mm-wide slabs, consisting of
260 extruded polystyrene doped with 1.5% paraterphenyl (PTP) and 0.01% POPOP. They were
261 cut to size then covered with a 30-100 μm thick diffuse reflector resulting from etching of
262 the surface with a chemical agent [9, 10]. The horizontal counter size is $2880 \times 31 \times 7.5 \text{ mm}^3$,
263 with one groove along the length of the bar in which sits a wavelength shifting fiber from
264 Kuraray. The vertical counter size is $1950 \times 210 \times 7.5 \text{ mm}^3$, with one U-shaped groove
265 along the bar. On each counter, two custom connectors house silicon photomultipliers,
266 MPPC type S12571-025C from Hamamatsu, either side of the horizontal counter, and
267 both connectors at the top for the vertical counter. This geometrical configuration for
268 vertical counters was chosen for ease of connectivity to the electronics, and maintenance
269 operations.

270 A total of 1744 horizontal counters and 315 vertical counters (including spares) were
271 produced at the Uniplast company (Vladimir, Russia).

272 **2.3.3 Electronics**

273 The Baby MIND electronic readout scheme includes several custom-designed boards [11].
274 The revised version is shown in Fig. 13. At the heart of the system is the electronics
275 Front End Board (FEB), developed by the University of Geneva. The readout system
276 includes two ancillary boards, the Backplane, and the Master Clock Board (MCB) whose
277 development has been managed by INRNE (Bulgarian Academy of Sciences) collaborators.

278 The FEBv2 hosts 3 CITIROC chips that can each read in signals from 32 SiPMs [6].
279 Each signal input is processed by a high gain, and a separate low gain, signal path. The
280 outputs from the slow shapers can be sampled using one of two modes: a mode with an
281 externally applied delay, and a peak detector mode. A faster shaper can be switched to

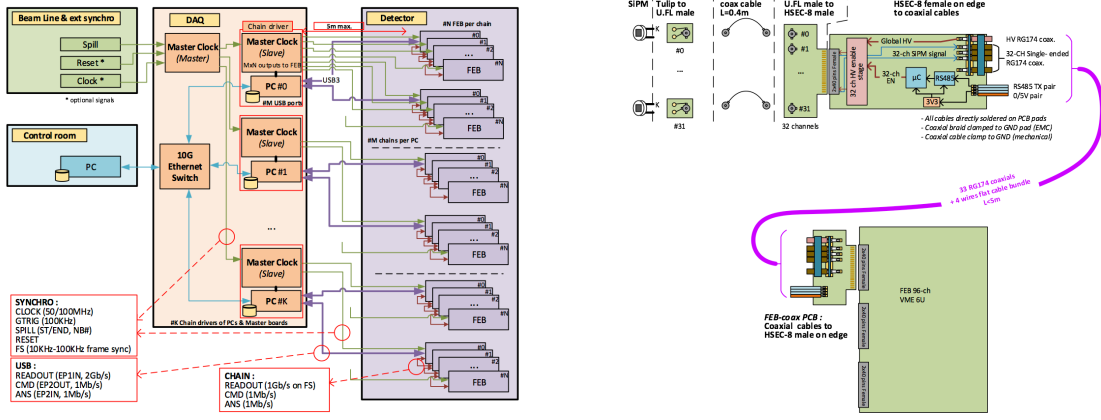


Figure 13: Left) Baby MIND electronics readout scheme. Right) SiPM-to-FEB connectivity.

either HG or LG paths, followed by discriminators with adjustable thresholds providing 32 individual trigger outputs and one OR32 trigger output. An Altera ARIA5 FPGA on the FEBv2 samples these trigger outputs at 400 MHz, recording rising and falling times for the individual triggers and assigning time stamps to these. Time-over-threshold from the difference between falling and rising times gives some measure of signal amplitude, used in addition to charge information and useful if there is more than one hit per bar within the deadtime due to the readout of the multiplexed charge output of $\sim 9 \mu\text{s}$. The ARIA5 also manages the digitization of the sampled CITIROC multiplexed HG and LG outputs via a 12-bit 8-ch ADC.

The internal 400 MHz clock on the FEBv2 can be synchronized to a common 100 MHz clock. The synchronization subsystem combines input signals from the beam line into a digital synchronization signal (SYNC) and produces a common detector clock (CLK) which can eventually be synchronised to an external experiment clock. Both SYNC and CLK signals are distributed to the FEBs. Tests show the FEB-to-FEB CLK(SYNC) delay difference to be 50 ps (70 ps). Signals from the beam line at WAGASCI include two separate timing signals, arriving 100 ms and 30 μs before the neutrino beam at the near detectors. The spill number is available as a 16-bit signal.

2.3.4 Pefromance check

All counters were measured at INR Moscow with a cosmic ray setup using the same type S12571-025C MPPCs and CAEN DT5742 digitizer. The average light yield (sum from both ends) was measured to be 37.5 photo-electrons (p.e.) per minimum ionizing particle (MIP) and 65 p.e./MIP for vertical and horizontal counters, respectively. After shipment to CERN, all counters were tested once more individually with an LED test setup [?]. 0.1% of

305 counters failed the LED tests and were therefore not used during the assembly of modules.
 306 The assembly of modules was completed in June 2017, and it was then tested in June and
 307 July 2017 at the Proton Synchrotron experimental hall at CERN with a mixed particle
 308 beam comprising mostly muons whose momenta could be selected between 0.5 and 5 GeV/c.
 An event display from the summer 2017 tests is shown in Fig. 14.

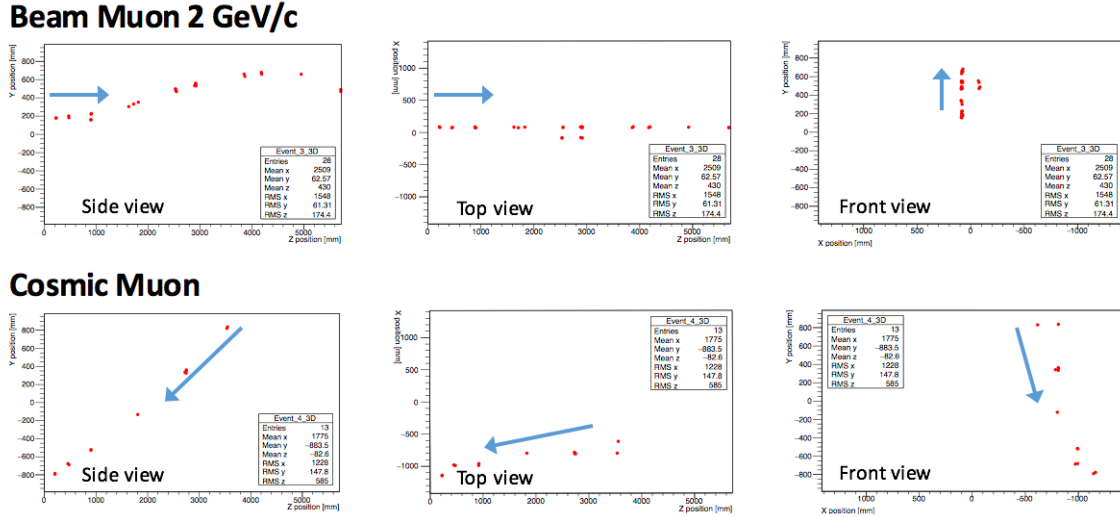


Figure 14: Comparison of a beam muon and cosmic muon in the three different geometrical projections of the detector. The beam impinges on the detector from the left. The arrows indicate the direction of travel of these muons. The direction of the cosmic muon is inferred from timing information.

309

310 2.4 Side muon range detector

311 Two Side-MRD modules for tracking secondary particles from neutrino interactions will be
 312 installed in 2018. Each Side-MRD module is composed of 11 steel plates and 10 layers of
 313 total 80 scintillator slabs installed in 13 mm gaps between the 30 mm thick plates. Each
 314 steel plate size is $30 \times 1610 \times 1800$ mm 3 . Total module size is $2236 \times 1630 \times 975$ mm 3 as
 315 shown in Fig. 15 (left), weight is ~ 8.5 ton.

316 Scintillator bars were manufactured by Uniplast company in Vladimir, Russia. Polystyrene
 317 based scintillators were extruded with thickness of 7 mm, then cut to the size of $7 \times 200 \times$
 318 1800 mm 3 . Dopant composition is 1.5% PTP and 0.01% POPOP. Scintillator surface was
 319 etched by a chemical agent to form a white diffuse layer with excellent reflective perfor-
 320 mance. Ideal contact between the scintillator and the reflector raises the light yield up to
 321 50% comparing to an uncovered scintillator. Sine like groove was milled along the scin-
 322 tillator to provide uniform light collection over the whole scintillator surface. WLS Y11

323 Kuraray fiber of 1 mm diameter is glued with an optical cement EJ-500 in the S-shape
 324 groove as shown in Fig. 15(right). Bending radius is fixed to 30 mm that was specified to
 325 be safe for Kuraray S-type fibers. Both ends of the fiber are glued into optical connectors
 326 which mounted within a scintillator body and provide an interface to SiPMs, Hamamatsu
 327 MPPC S13081-050CS(X1).

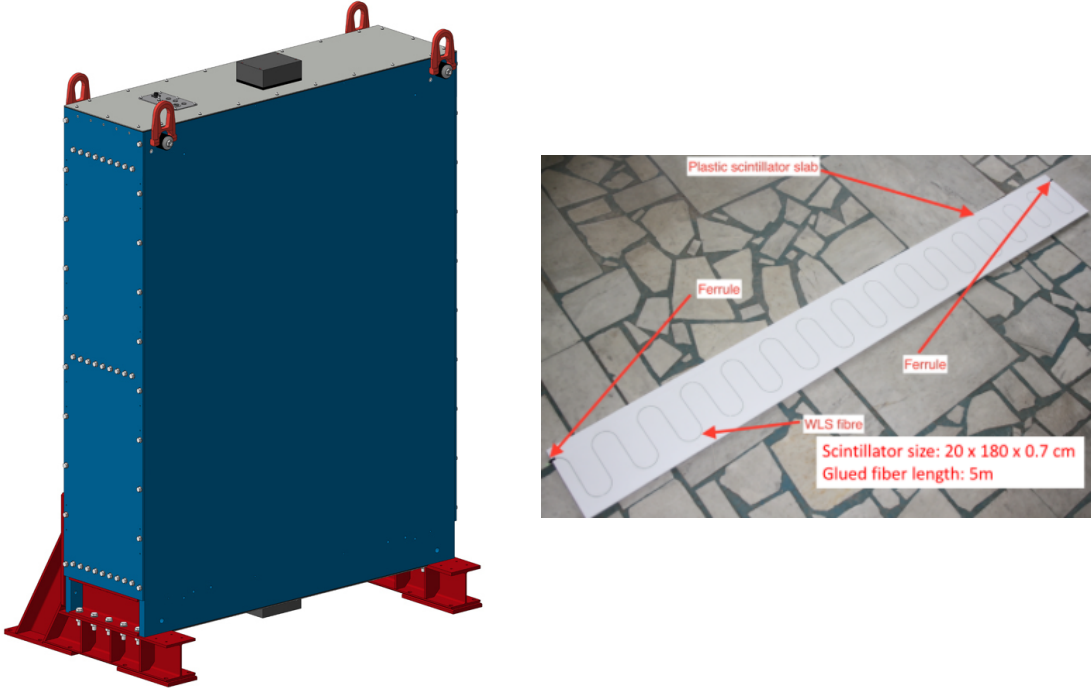


Figure 15: Left :Side-MRD module. Right: Scintillator bar of the Side-MRD modules.

328 Scintillators for the Side-MRD modules had been assembled at INR in Russia, and
 329 shipped to Japan in July 2017. The light yield for each scintillator was measured with
 330 cosmic rays at INR and at YNU in Japan after delivery. Parameters measured at the
 331 center of the counter were : the light yields LY_1 and LY_2 at both ends, the light yield
 332 asymmetry between the ends calculated as $100\% \times \frac{LY_1 - LY_2}{LY_1 + LY_2}$. After tests at INR we selected
 333 324 counters from measured 332 ones with the mean light yield of 45 p.e./MIP ($LY_1 + LY_2$
 334) and the asymmetry value less than 10 % . The measuremens at YNU yielded the average
 335 total light yield of about 40 p.e./MIP which varies in range from 32 to 50 p.e./MIP (Fig.
 336 16 (left)). Only two counters showed relatively high asymmetry close to 25 % as shown in
 337 Fig. 16 (right). Using the results of the quality assurance test we selected 320 scintillator
 338 counters for the Side-MRD modules.

339 We also measured the time resolution for a combination of four counters piled each on
 340 another one. The average result for four counters is $\sigma_T = 1.04$ ns. The resolution of com-
 341 bination of 2, 3, 4 counters is measured to be 0.79 ns, 0.66 ns and 0.58 ns, correspondently.

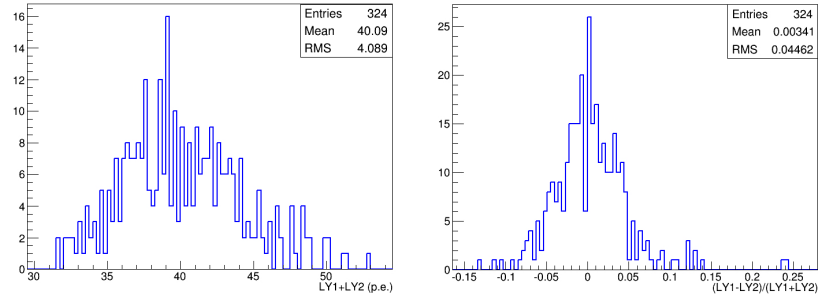


Figure 16: Total light yield distribution (left) and light yield assymetry (right) measured at YNU.

342
 343 Construction of Side-MRD modules will be done from November 2017 at Yokohama
 344 National University, then they will be transported to J-PARC and will be installed at B2
 345 floor of the T2K near detector hall.

346 Same electronics as the WAGASCI modules (see Sec. 2.1.2) are used for the Side-MRD
 347 modules.

348 3 Physics goals

349 We will measure the differential cross section for the charged current interaction on H₂O
 350 and Hydrocarbon(CH)). The water-scintillator mass ratio of the Wagasci module is as
 351 high as 5:1 and the high purity measurement of the cross section on H₂O is possible. One
 352 experimental option is to remove water from one of the two Wagasci modules. The water-
 353 out WAGASCI module will allow to measure pure-CH target interactions with very low
 354 momentum-threshold for protons. It will also benefit to subtract the background from
 355 interaction with scintillator in the water target measurement. Another option is to add
 356 the T2K proton module which is fully made of plastic scintillators. It will allow the high
 357 statistics comparison of cross section between H₂O and CH and also comparison with
 358 the ND280 measurement. The actual configuration will be optimized with detailed MC
 359 simulation by 2018 Summer.

360 Our setup allows the measurements of inclusive and also exclusive channels such as 1- μ ,
 361 1- $\mu 1p$, 1- $\mu 1\pi \pm np$ samples, former two of which are mainly caused by the quasi-elastic and
 362 2p2h interaction and the latter is mainly caused by resonant or coherent pion production

and deep elastic scattering. In general, an accelerator produced neutrino beam spectrum is wide and the energy reconstruction somehow rely on the neutrino interaction model. Therefore, recent neutrino cross section measurement results including those from T2K are given as a flux-integrated cross section rather than cross sections as a function of the neutrino energy to avoid the model dependency. We can provide the flux-averaged cross section. In addition, by combining our measurements with those at ND280, model-independent extraction of the cross section for narrow energy region becomes possible. This method was demonstrated in [1] and also proposed by P** (NUPRISM).

3.1 Expected number of events

Expected number of neutrino events after the event selections is evaluated with Monte Carlo simulations as we will discuss in Section 5. In the neutrino-mode, 4.2×10^3 , 1.1×10^3 and 3.8×10^3 CC neutrino events are expected in the water-in WAGASCI module, the water-out WAGASCI module and the INGRID proton module after the selections with 0.5×10^{21} POT, and its purities are 78.0 %, 97.5 % and $\sim 98\%$. In the antineutrino-mode, 1.7×10^3 , 0.4×10^3 and 1.5×10^3 CC antineutrino events are expected in the water-in WAGASCI module, the water-out WAGASCI module and the INGRID proton module after the selections with 0.5×10^{21} POT, and its purities are 59.5 %, 74.4 % and $\sim 74\%$.

Statistical errors of flux integrated CC-inclusive neutrino cross section measurements on H₂O (full acceptance) and CH targets (forward acceptance) will be 1.5 % and 1.6 % with 0.5×10^{21} POT in the neutrino-mode. Statistical errors of flux integrated CC-inclusive antineutrino cross section measurements on H₂O (full acceptance) and CH targets (forward acceptance) will be 2.4 % and 2.5 % with 0.5×10^{21} POT in the antineutrino-mode.

Statistical errors of flux integrated H₂O to CH CC-inclusive neutrino cross section ratio measurement will be 3.1 % (full acceptance) and 2.3 % (forward acceptance) with 0.5×10^{21} POT in the neutrino-mode. Statistical errors of flux integrated H₂O to CH CC-inclusive antineutrino cross section ratio measurement will be 5 % (full acceptance) and 3.7 % (forward acceptance) with 0.5×10^{21} POT in the antineutrino-mode.

3.2 Pseudo-monochromatic beam by using different off-axis fluxes

The off-axis method gives narrower neutrino spectrum, and the peak energy is lower for larger off-axis angle. There still remains high energy tail mainly due to neutrinos from Kaon decay. The off-axis angle of the Wagasci location is 1.5 degree and different from the ND280 2.5 degree. Top two plots of Fig. 17 show the energy spectra of fluxes and neutrino interaction events at these two different locations. The high energy tail of ND280 flux can be somehow subtraction by using the Wagasci measurement. The low energy part of the Wagasci flux can be also subtracted by using the ND280 measurement. Bottom two plots of Fig. 17 demonstrate this method. We can effectively get two fluxes, from 0.2 GeV to 0.9 GeV and 0.6 GeV and 2 GeV and measure flux-integrated cross section for these two

400 fluxes.

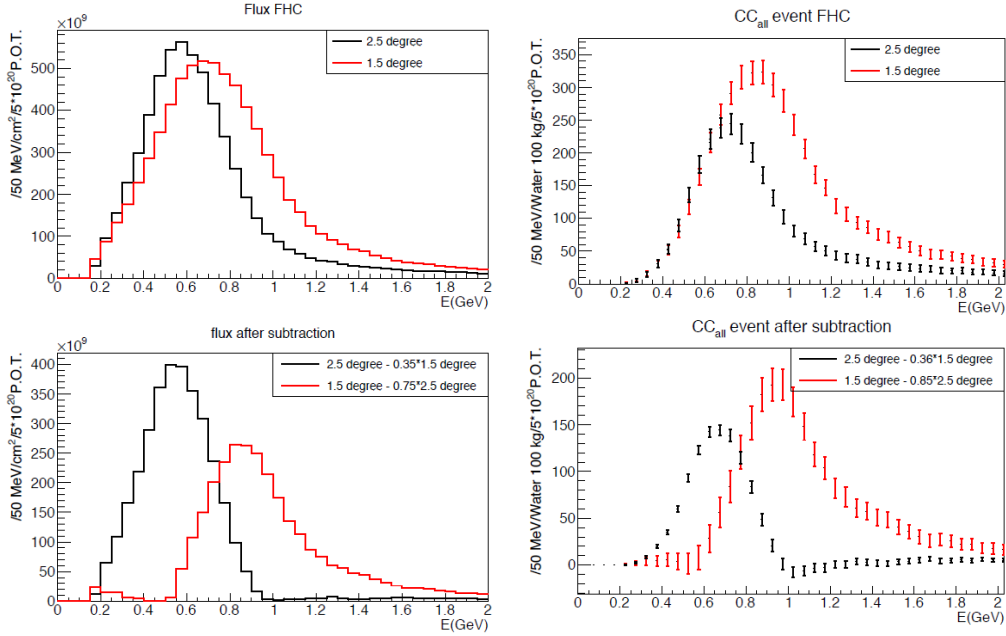


Figure 17: Energy spectra obtained by using different off-axis angle fluxes. Top two plots show the fluxes(left) and spectra of interaction events (right) for ND280 (off-axis 2.5 degree) and Wagasci (off-axis 1.5 degree). Bottom two plots show the fluxes (left) and spectra of interaction events (right) obtained by subtraction of fluxes at ND280 and Wagasci. The error bar is for the statistical error and those in the bottom right plot is obtained assuming the statistical error for ND280 measurement is much smaller than that of Wagasci experiment.

401 Statical errors of flux integrated CC-inclusive neutrino cross section measurements
 402 on H₂O (forward acceptance) and CH targets (forward acceptance) with the pseudo-
 403 monochromatic beam will be 2 % and 1.9 % with 0.5×10^{21} POT in the neutrino-mode.
 404 Statical errors of flux integrated CC-inclusive antineutrino cross section measurements
 405 on H₂O (forward acceptance) and CH targets (forward acceptance) with the pseudo-
 406 monochromatic beam will be 3 % and 2.8 % with 0.5×10^{21} POT in the neutrino-mode.

407 3.3 Subjects Wagasci can contribute

408 In T2K experiment, neutrinos interact with bound nucleons in relatively heavy nuclei
 409 (Carbon and Oxygen), so the cross-section is largely affected by nuclear effects. The nuclear
 410 effects are categorized as nucleons' momentum distribution in nucleus, interactions with

411 correlated pairs of nucleons in nucleus (two particles-two holes, 2p2h), collective nuclear
 412 effects and final state interactions (FSI) of secondary particles in the nuclei after the initial
 413 neutrino interactions.

414 The 2p2h interactions mainly happen through Δ resonance interactions following a
 415 pion-less decay and interactions with a correlated nucleon pair. The 2p2h interactions are
 416 observed in electron scattering experiments [7] where the 2p2h events observed in the gap
 417 between Quasi-Elastic region and Pion-production region as shown in Fig. 18. Neutrino
 418 experiments also attempt to measure the 2p2h interactions, but separation of the QE peak
 419 and the 2p2h peak is more difficult because transferred momentum (p) and energy (w)
 420 are largely affected by neutrino energies which cannot be determined event-by-event in the
 421 wide energy spectrum of the accelerator neutrino beam. Our model-independent narrow
 422 neutrino spectra extracted from combined analyses of our data and ND280 data are ideal
 423 for searching the 2p2h interaction because clearer separation of the QE peak and the 2p2h
 424 peak is expected. Another way to observe the 2p2h interaction is direct measurement of
 425 proton tracks in CC0 π sample with low detection threshold and full acceptance. Fig. 19
 426 shows proton multiplicities after FSI in CCQE events and 2p2h events, and Fig. 19 shows
 427 opening angles among two proton tracks in the same samples. The water-out Wagasci
 428 can provide good sample for the 2p2h interaction search because its low density medium
 429 enables the detection of low momentum protons in addition to the full acceptance.

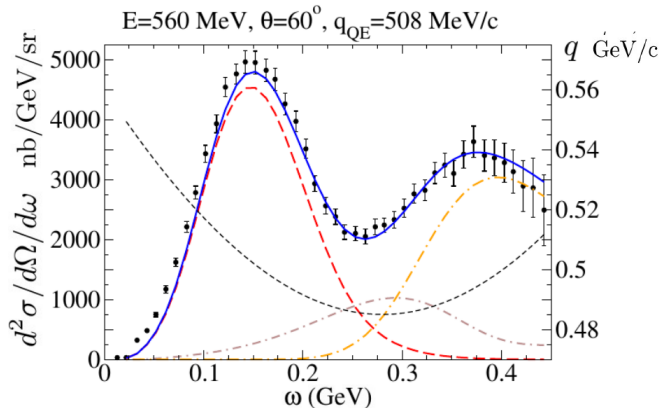


Figure 18: Comparison of inclusive $^{12}\text{C}(\text{e},\text{e}')$ cross sections and predictions of the QE-SuSAv2 model (long-dashed red line), 2p-2h MEC model (dot-dashed brown line) and inelastic-SuSAv2 model (long dot-dashed orange line) (from Ref. [7]). The sum of the three contributions is represented with a solid blue line. The q dependence with ω is also shown (short-dashed black line.)

430 There are various models which describe the collective nuclear effects [8]. The Q^2
 431 dependence of the effects can be tested by measuring angular distribution of muons in

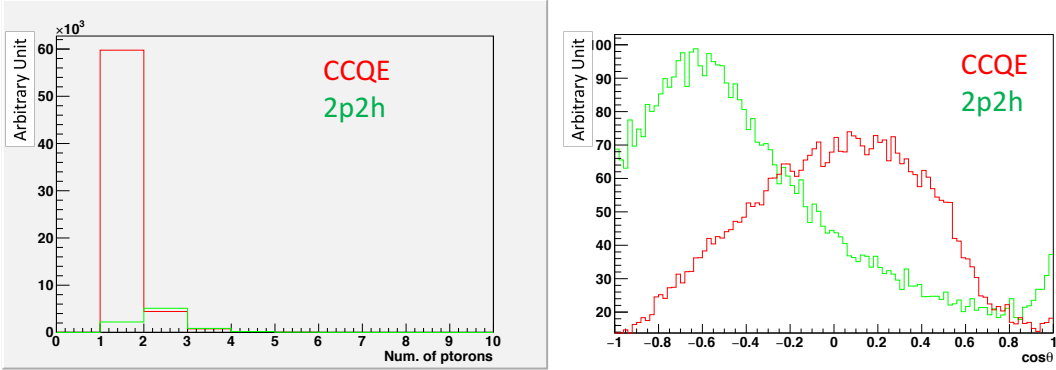


Figure 19: Proton multiplicities (left) and opening angles among two proton tracks (right) after FSI in CCQE events and 2p2h events.

432 CC1- μ and CC1- $\mu 1p$ events. The uncertainties of the effects in low (high) Q^2 regions can
 433 be constrained by observing the events with a forward-going (high-angle) muon, so it is
 434 essential to measure muon tracks with full acceptance.

435 T2K experiment is starting to use ν_e CC1 π events for its CP violation search to increase
 436 the statistics. One of the biggest uncertainty of the CC1 π sample comes from the final
 437 state interactions of pions in the nuclei after the initial neutrino interactions because they
 438 change the multiplicity, charge and kinematics of the pions. The multi-pion production
 439 events can be migrated into the CC1 π sample due to the FSIs, and they become important
 440 backgrounds. We can constrain the uncertainties from the pion FSIs by measuring pion
 441 rescattering in the detector and pion multiplicity in ν_μ CCn π sample with low detection
 442 threshold and full acceptance for pion tracks. The water-out WAGASCI can provide good
 443 sample for the pion FSI studies because its low density medium enables the detection of
 444 low momentum pions in addition to the full acceptance.

4 Status of J-PARC T59 experiment

446 We had submitted a proposal of a test experiment to J-PARC in April 2014 to test a new
 447 detector with a water target, WAGASCI, at the neutrino monitor hall, and the proposal
 448 was approved as J-PARC T59. The project contains the side and downstream muon range
 449 detectors as well.

450 The first WAGASCI module has been constructed in 2016 and installed at the on-
 451 axis position in front of the T2K INGRID detector for the commissioning and the first
 452 cross section measurement as a part of the T2K experiment. The INGRID electronics
 453 boards are used to read the signal. The light yield measured with muons produced by

454 the interaction of neutrinos in the hall wall, shown in Fig. 20, is sufficiently high to get
455 good hit efficiency. A track search algorithm based on the cellular automaton has been

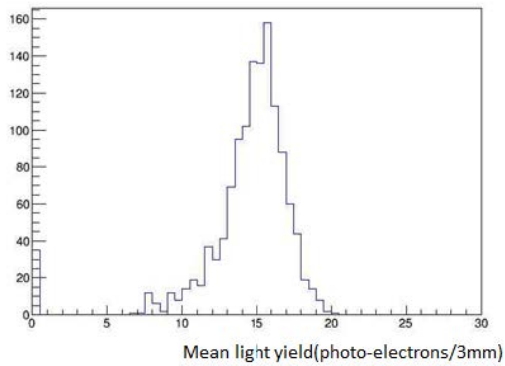


Figure 20: Light yield for muons produced by the interaction of neutrinos in the hall wall. Average light yields for each channel are plotted.

455
456 developed using the software tools by the T2K INGRID. Examples of observed events are
457 shown in Fig. 21 The tracking efficiency in 2-dimensional projected plane was evaluated
458 by comparing the reconstructed track in the WAGASCI module and the INGRID module
459 and shown in Fig.22. Note that that the tracking efficiency for high angle (> 70 deg) is not
460 evaluated because of the acceptance of the INGRID module, not because of the limitation
461 of the WAGASCI module.

462 In 2017 Autumn, the construction of the second WAGASCI module and the dedicated
463 electronics board were completed. The module and the electronics were install to the B2
464 floor together with the T2K proton module and the INGRID module as shown in Fig. 23.
465 The proton module is to be used as the entering muon veto and also for the comparison
466 of interaction between CH and Water. The INGRID module is for the temporary muon
467 detector with limited acceptance for this period. The detector was commissioned and is
468 in operation to take data with the antineutrino beam during the T2K beam time from
469 October.

470 The production of the components of the side muon range detectors has been completed
471 and now the detectors are being assembled at the Yokohama National University. These
472 detectors will be installed sometime from January to June, 2018 when T2K is not running.

473 The Baby MIND detector was transported from CERN to Japan in December, 2017.
474 It will be installed and commissioned in Jan.-Feb. 2018 and T59 will take the neutrino-
475 induced muon data in April and May.

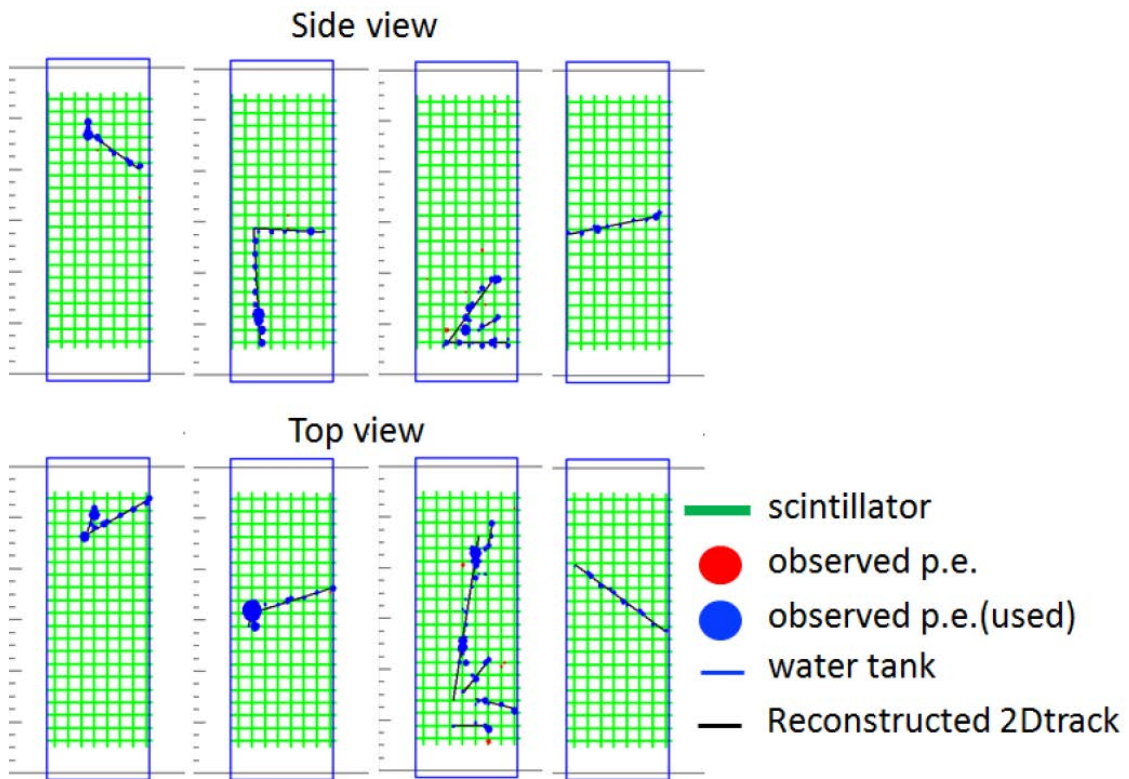


Figure 21: Example event displays of the WAGASCI module at on-axis. The reconstructed tracks are overlaid.

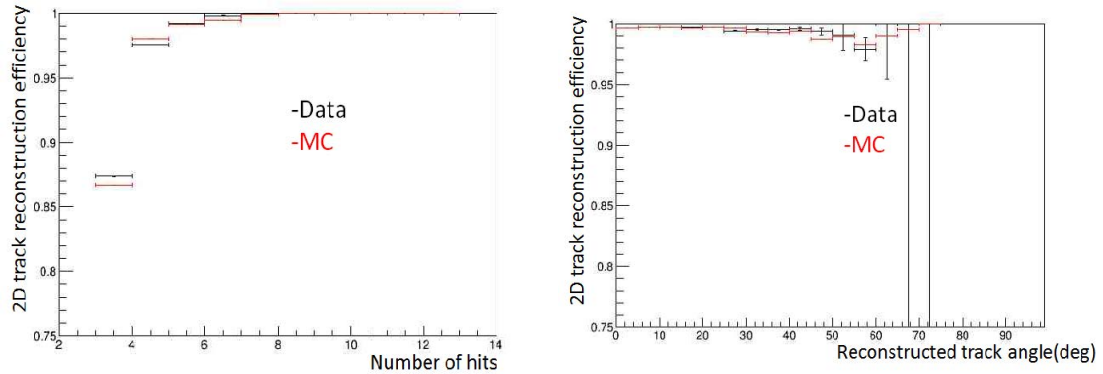


Figure 22: 2D track reconstruction efficiency as a function of number of hits (left) and track angle (right). Here the track angle is the one reconstructed by the INGRID module.

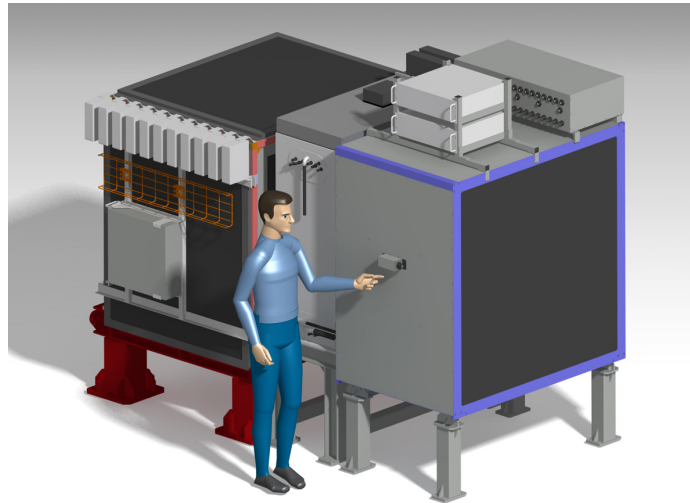


Figure 23: J-PARC T59 detector configuration in October 2017.

476 **5 MC studies**

477 **5.1 Detector simulation**

478 Expected number of neutrino events in the water-in Wagasci detector is evaluated with
479 Monte Carlo simulations. Neutrino beam flux at the detector location is simulated by
480 T2K neutrino flux generator, JNUBEAM, neutrino interactions with target materials are
481 simulated by a neutrino interaction simulator, NEUT, detector responses are simulated
482 using GEANT4-based simulation. The neutrino flux at the detector location, 1.5 degrees
483 away from the J-PARC neutrino beam axis, is shown in Figure 4, and its mean neutrino
484 energy is around 0.68 GeV.

485 **5.1.1 Detector geometry**

486 The detector geometry in the GEANT4-based simulation is slightly different from the actual
487 detector as shown in Fig. 24. The active neutrino target region consists of four Wagasci
488 modules, and each Wagasci detector has the dimension with 100 cm × 100 cm in the x and
489 y directions and 50 cm along the beam direction. Two Side-MRD modules is installed at
490 both sides of the Wagasci modules, and each Side-MRD module consists of ten iron plates
491 whose dimension is 3 cm (thickness) × 200 cm (height) × 320 cm (width). The distance
492 between the Side-MRD modules and Wagasci modules is 80 cm. The downstream-MRD
493 equivalent to the Baby-MIND is installed at the downstream of the Wagasci modules. The
494 downstream-MRD consists of thirty iron plates whose dimension is 3 cm (thickness) × 200
495 cm (height) × 400 cm (width). The distance between the downstream-MRD modules and
496 Wagasci modules is 80 cm.

497 **5.1.2 Response of detector components**

498 The energy deposit inside the scintillator is converted into the number of photons. The
499 effects of collection and attenuation of the light in the scintillator and the WLS fiber are
500 simulated, and the MPPC response is also taken into account. The light yield is smeared
501 according to statistical fluctuations and electrical noise.

502 **5.2 Track reconstruction**

503 To select neutrino interaction from the hit patterns, a track reconstruction algorithm is
504 developed. The flow of the track reconstruction is as follows.

- 505 1. Two-dimensional track reconstruction in each sub-detectors
506 2. Track matching among the sub-detectors
507 3. Three -dimensional track reconstruction
508 Add explanation about two-dim reco, track matching and three-dim reco here.

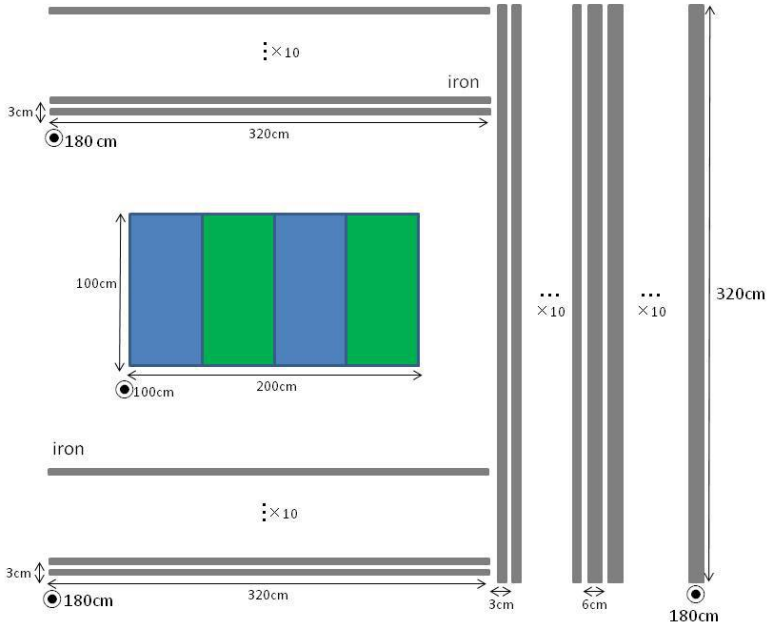


Figure 24: Geometry of the detectors in the Monte Carlo simulation.

509 5.3 Event selection

510 First, the events with the track which starts in 5 cm from the wall of the Wagasci module
 511 are rejected to remove the background from the outside.

512 Second, to reject backgrounds from NC and neutral particles, the longest tracks are
 513 required to penetrate more than one (five) iron plates in Side-MRD modules (Baby-MIND).
 514 Then, in order to measure muon momentum, the longest tracks are required to stop in
 515 MRDs (Side-MRD modules and Baby-MIND) or penetrate all iron plates.

516 Table 1 and 2 show numbers of the selected events in one water-in Wagasci module
 517 after each event selection in neutrino-mode and antineutrino-mode respectively. As for
 518 the neutrino-mode, 8478 CC events are expected with 1×10^{21} POT, and the purity is
 519 78.0 %. The main background for the neutrino-mode is the neutrino interactions in the
 520 scintillators inside the Wagasci detector. As for the antineutrino-mode, 3331 CC events
 521 are expected with 1×10^{21} POT, and the purity is 59.5 %. The main background for the
 522 antineutrino-mode is the wrong sign contamination from ν_μ events and the antineutrino
 523 interactions in the scintillators inside the Wagasci detector.

524 Table 3 and 4 show numbers of the charged-current events in the water-in Wagasci
 525 module after all event selection with a classification based on interactions at a vertex with

Table 1: Expected number of the neutrino-candidate events in one water-in Wagasci module with 1×10^{21} POT in neutrino-mode.

Cut	CC	NC	Scinti Bkg.	Total
Reconstructed	18093.2	699.7	4698.3	23491.2
FV	15150.8	588.4	3934.8	19673.9
Pene. iron	11264.3	237.3	2875.4	14377.0
Stop/Penetrate MRDs	8478.2	214.0	2173.1	10865.2
after all cuts	78.0 %	2.0 %	20.0 %	100 %

Table 2: Expected number of the antineutrino-candidate events in one water-in Wagasci module with 1×10^{21} POT in antineutrino-mode.

Cut	CC	NC	Scinti Bkg.	Wrong sign bkg	Total
Reconstructed	6499.7	107.3	2234.4	2330.8	11172.1
FV	5457.9	89.3	1873.5	1946.6	9367.1
Pene. iron	4172.3	30.8	1440.9	1560.6	7204.6
Stop/Penetrate MRDs	3331.5	28.5	1120.3	1121.2	5601.5
after all cuts	59.5 %	0.5 %	20.0 %	20.0 %	100 %

526 1×10^{21} POT in neutrino-mode and antineutrino-mode respectively.

Table 3: Expected number of the charged-current events in the water-in Wagasci module after the event selections with 1×10^{21} POT in neutrino-mode with a classification based on interactions at a vertex.

CCQE	MEC	CCRes	CCDIS	Total
3716.3	747.0	2081.3	1132.3	7676.9
48.4 %	9.7 %	27.1 %	14.7 %	100 %

527 Table 5 and 6 show numbers of the charged-current events in one water-in Wagasci
528 module after all event selection with a classification based on particles after final state
529 interactions with 1×10^{21} POT in neutrino-mode and antineutrino-mode respectively.

530 Figure 25 shows the reconstructed angles of the longest tracks in the selected events in
531 the neutrino-mode and the anti-neutrino mode. Figure ?? shows the iron plane numbers
532 in Side-MRD and Baby-MIND corresponding to the end points of the longest tracks in the
533 selected events in the neutrino-mode and the anti-neutrino mode.

Table 4: Expected number of the charged-current events in the water-in Wagasci module after the event selections with 1×10^{21} POT in antineutrino-mode with a classification based on interactions at a vertex.

CCQE	MEC	CCRes	CCDIS	Total
2522.0	362.8	765.8	765.8	4416.4
hline 57.1 %	8.2 %	17.3 %	17.3 %	100 %

Table 5: Expected number of the charged-current events in one water-in Wagasci module after the event selections with 1×10^{21} POT in neutrino-mode with a classification based on particles after final state interactions.

CC0 π	CC1 π	CC2 π	CCn π	Total
5423.1	1684.3	242.9	701.1	8051.4
67.4 %	20.9 %	3.0 %	8.7 %	100 %

534 5.4 Cross section measurements

535 The flux-averaged ν_μ ($\bar{\nu}_\mu$) CC inclusive cross sections on water and hydrocarbon are calcu-
 536 lated from the number of selected events using the background subtraction and efficiency
 537 correction

$$\sigma_{CC} = \frac{N_{sel} - N_{BG}}{\phi T \epsilon}, \quad (1)$$

538 where N_{sel} is the number of selected events from real data, N_{BG} is the number of selected
 539 background events predicted by MC simulation, ϕ is the integrated ν_μ flux, T is the number
 540 of target nucleons, and ϵ is the detection efficiency for CC events predicted by MC simula-
 541 tion. in the water and hydrocarbon regions in the central detector. Finally, we will cancel
 542 the dominant systematic error, the neutrino flux error, by comparing the cross-section re-
 543 sults from two neutrino targets, water and hydrocarbon, having almost identical neutrino
 544 fluxes, and measure the water to hydrocarbon charged current cross section ratio with 3%

Table 6: Expected number of the charged-current events in one water-in Wagasci module after the event selections with 1×10^{21} POT in antineutrino-mode with a classification based on particles after final state interactions.

CC0 π	CC1 π	CC2 π	CCn π	Total
2529.3	520.0	37.9	96.0	3183.2
79.5 %	16.3 %	1.2 %	3.0 %	100 %

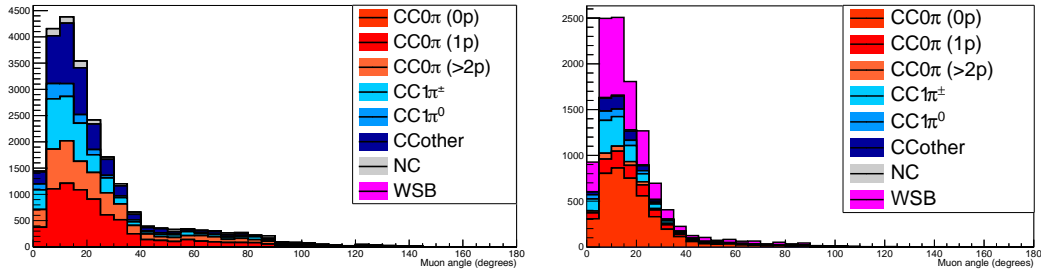


Figure 25: The reconstructed angles of the longest tracks in the selected events in the neutrino-mode (left) and the antineutrino-mode (right).

precision, which is achieved in the INGRID measurement [4].

In the water target events, the background from interaction with scintillators has to be subtracted by using the measurement of the hydrocarbon target.

6 Standalone WAGASCI-module performances

In the previous sections, the WAGASCI detector was studied using the Muon Range Detectors. In this section, the standalone abilities of WAGASCI module are presented. Using the WAGASCI configuration presented in Section 5, we have evaluated that only 7% of the muons will be stopped in one of the WAGASCI modules. THowerver, this proportion increases to 53% for pions and 73% for protons produced by neutrino interactions at 1.5° off-axis. Figure 27 shows the momentum distribution of these daughter particles as well as for the sub-sample stopped in one of the WAGASCI modules. Therefore, the study of the standalone abilities of the WAGASCI module in this section are dominantly motivated by:

- the accurate measurement of the neutrino interaction final states. Though most of the muons will be reconstructed and identified in the MRDs, the hadronic particles will predominantly stops in one WAGASCI module. One has therefore to rely exclusively on the WAGASCI module information alone to reconstruct, identify and measure the momentum of pions or protons.
- the coverage of the MRDs is not 4π . Using the WAGASCI module information can therefore help to constraint the particles that exits the WAGASCI module but do not geometrically enters any MRD.
- the particle identification of low momenta muons $p_\mu < 300 \text{ MeV}/c$ that will leave only few hits in the MRD. Using the WAGASCI module information will clearly enhance the particle identification.

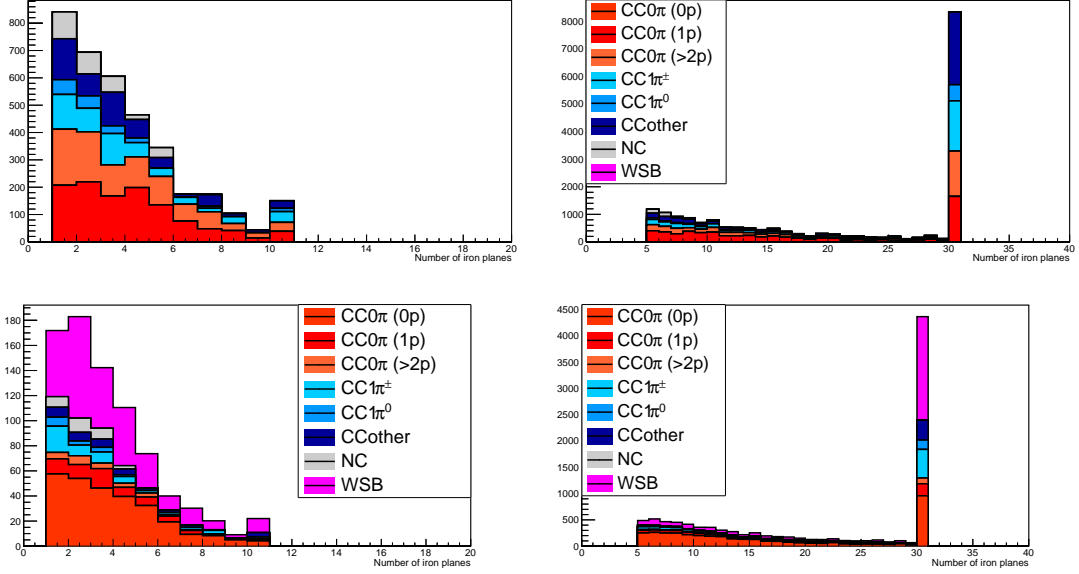


Figure 26: Iron plane numbers in Side-MRD (left) and Baby-MIND (right) corresponding to the end points of the longest tracks in the selected events in the neutrino-mode (top) and the antineutrino-mode (bottom).

568 This study is based on an original study done for the ND280 upgrade target, with some
 569 modifications. Though the cell size is similar to the WAGASCI configuration presented
 570 in Section 5, the external dimensions are different ($186.4 \times 60 \times 130 \text{ cm}^3$). Whenever the
 571 results are presented with this external size and this parameter is likely to impact the
 572 result, it will be mentioned.

573 Note that in this section, a simplified reconstruction algorithm presented in Section 6.1 is
 574 used. The fiducial volume is chosen accordingly as the inner cube of the module which
 575 surfaces are distant of $4 \times$ scintillator space = 10 cm from the module external surfaces.
 576 The neutrino interactions are simulated using NEUT v5.3.2. The NEUT input neutrino
 577 flux is estimated using JnuBeam v13a and assuming the detector to be located at 1.5°
 578 off-axis, as in Section 5. Note that the event reconstruction efficiency as a function of true
 579 neutrino energy might be changed at 1.5° , due for example to different Q^2 distributions. For
 580 this reason, one has to note that the reconstruction results might slightly be changed from
 581 2.5° and 1.5° . To avoid a similar change on the particle-only reconstruction efficiencies,
 582 they will be presented as a function of variables that completely characterize the particle
 583 kinematic state, *i.e.* its momentum and angle. Figure 28 shows the vertices distributions
 584 of the daughter particles of neutrinos interacting one standard WAGASCI water-module.
 585 In this section, we will show the detector reconstruction and particle identification in this

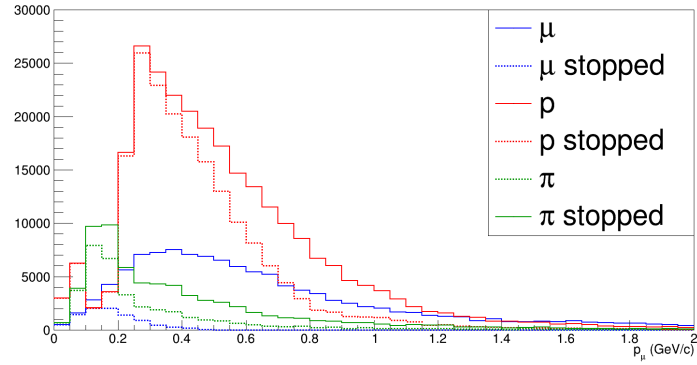


Figure 27: Momentum distribution of true particles in WAGASCI (plain) and corresponding distributions only for particles stopping into the WAGASCI module (dashed).

586 phase space, both for leptonic and hadronic particles. We will finally show an empty
 587 WAGASCI module can highly enhance the ability to constrain the neutrino interaction
 588 final state which is critical to reduce the corresponding uncertainties.

589 6.1 Reconstruction algorithm

590 6.1.1 Description

591 For this section, an ideal “simulated” reconstruction is developed. A particle is recon-
 592 structed if:

- 593 1. The particle is charged.
- 594 2. Lets at least one hit (energy deposit > 2.5 photo-electron) in a scintillator.
- 595
- 596 3. The particle enters one TPC and let one hit in the tracker.

597 Or

598

- 599 • The particle should be long enough to be reconstructed by the detector in at
 600 least 2 out of 3 views (XZ, YZ, XY). The length criterion requires the particle
 601 to let at least 4 hits in the detector. In the “less favourable case” of pure
 602 longitudinal or transverse going tracks, it represents a the track length of $L_{track} \geq$
 603 $4 \times$ scintillator space = 10.0 cm.
- 604 • In the views where particles pass the length criterion, the particle shall not
 605 be superimposed with longer tracks in at least two views. The superposition
 606 criterion is estimated with the distance inter-tracks (DIT) which corresponds to

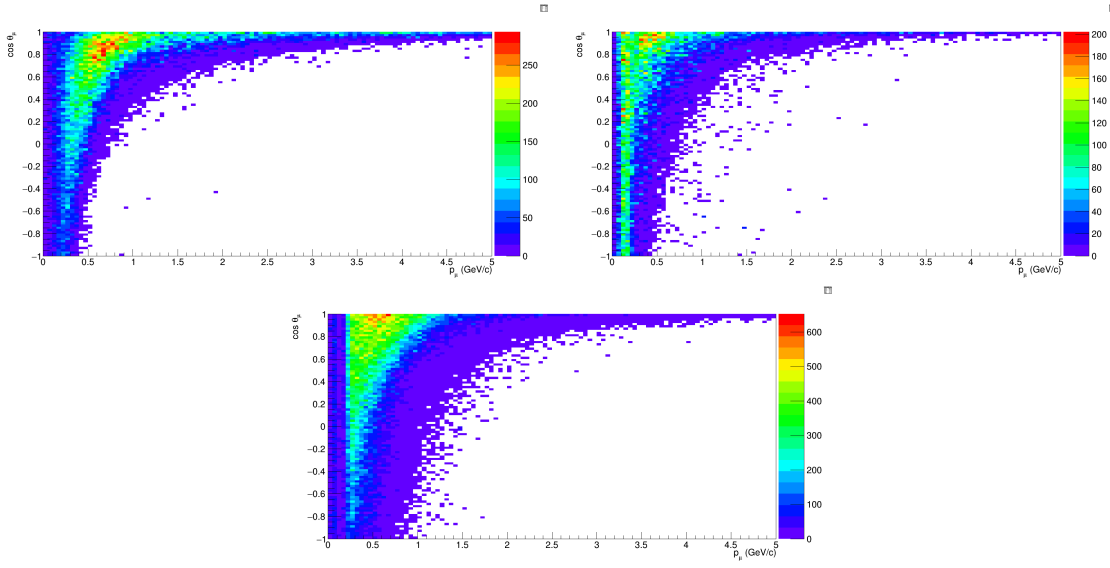


Figure 28: True number of muons (left), charged pions (right) and protons (bottom) in the two WAGASCI water-module as a function of the particles momenta and angles at 1.5° .

607
 608
 609
 610
 611
 612
 613
 the orthogonal distance between two tracks at the ending point of the shortest
 607
 608
 609
 610
 611
 612
 613
 614
 615
 616
 617
 618
 619
 620
 621
 622
 623
 624
 625
 626
 627
 628
 629
 630
 631
 632
 633
 634
 635
 636
 637
 638
 639
 640
 641
 642
 643
 644
 645
 646
 647
 648
 649
 650
 651
 652
 653
 654
 655
 656
 657
 658
 659
 660
 661
 662
 663
 664
 665
 666
 667
 668
 669
 670
 671
 672
 673
 674
 675
 676
 677
 678
 679
 680
 681
 682
 683
 684
 685
 686
 687
 688
 689
 690
 691
 692
 693
 694
 695
 696
 697
 698
 699
 700
 701
 702
 703
 704
 705
 706
 707
 708
 709
 710
 711
 712
 713
 714
 715
 716
 717
 718
 719
 720
 721
 722
 723
 724
 725
 726
 727
 728
 729
 730
 731
 732
 733
 734
 735
 736
 737
 738
 739
 740
 741
 742
 743
 744
 745
 746
 747
 748
 749
 750
 751
 752
 753
 754
 755
 756
 757
 758
 759
 760
 761
 762
 763
 764
 765
 766
 767
 768
 769
 770
 771
 772
 773
 774
 775
 776
 777
 778
 779
 780
 781
 782
 783
 784
 785
 786
 787
 788
 789
 790
 791
 792
 793
 794
 795
 796
 797
 798
 799
 800
 801
 802
 803
 804
 805
 806
 807
 808
 809
 810
 811
 812
 813
 814
 815
 816
 817
 818
 819
 820
 821
 822
 823
 824
 825
 826
 827
 828
 829
 830
 831
 832
 833
 834
 835
 836
 837
 838
 839
 840
 841
 842
 843
 844
 845
 846
 847
 848
 849
 850
 851
 852
 853
 854
 855
 856
 857
 858
 859
 860
 861
 862
 863
 864
 865
 866
 867
 868
 869
 870
 871
 872
 873
 874
 875
 876
 877
 878
 879
 880
 881
 882
 883
 884
 885
 886
 887
 888
 889
 890
 891
 892
 893
 894
 895
 896
 897
 898
 899
 900
 901
 902
 903
 904
 905
 906
 907
 908
 909
 910
 911
 912
 913
 914
 915
 916
 917
 918
 919
 920
 921
 922
 923
 924
 925
 926
 927
 928
 929
 930
 931
 932
 933
 934
 935
 936
 937
 938
 939
 940
 941
 942
 943
 944
 945
 946
 947
 948
 949
 950
 951
 952
 953
 954
 955
 956
 957
 958
 959
 960
 961
 962
 963
 964
 965
 966
 967
 968
 969
 970
 971
 972
 973
 974
 975
 976
 977
 978
 979
 980
 981
 982
 983
 984
 985
 986
 987
 988
 989
 990
 991
 992
 993
 994
 995
 996
 997
 998
 999
 1000
 1001
 1002
 1003
 1004
 1005
 1006
 1007
 1008
 1009
 1010
 1011
 1012
 1013
 1014
 1015
 1016
 1017
 1018
 1019
 1020
 1021
 1022
 1023
 1024
 1025
 1026
 1027
 1028
 1029
 1030
 1031
 1032
 1033
 1034
 1035
 1036
 1037
 1038
 1039
 1040
 1041
 1042
 1043
 1044
 1045
 1046
 1047
 1048
 1049
 1050
 1051
 1052
 1053
 1054
 1055
 1056
 1057
 1058
 1059
 1060
 1061
 1062
 1063
 1064
 1065
 1066
 1067
 1068
 1069
 1070
 1071
 1072
 1073
 1074
 1075
 1076
 1077
 1078
 1079
 1080
 1081
 1082
 1083
 1084
 1085
 1086
 1087
 1088
 1089
 1090
 1091
 1092
 1093
 1094
 1095
 1096
 1097
 1098
 1099
 1100
 1101
 1102
 1103
 1104
 1105
 1106
 1107
 1108
 1109
 1110
 1111
 1112
 1113
 1114
 1115
 1116
 1117
 1118
 1119
 1120
 1121
 1122
 1123
 1124
 1125
 1126
 1127
 1128
 1129
 1130
 1131
 1132
 1133
 1134
 1135
 1136
 1137
 1138
 1139
 1140
 1141
 1142
 1143
 1144
 1145
 1146
 1147
 1148
 1149
 1150
 1151
 1152
 1153
 1154
 1155
 1156
 1157
 1158
 1159
 1160
 1161
 1162
 1163
 1164
 1165
 1166
 1167
 1168
 1169
 1170
 1171
 1172
 1173
 1174
 1175
 1176
 1177
 1178
 1179
 1180
 1181
 1182
 1183
 1184
 1185
 1186
 1187
 1188
 1189
 1190
 1191
 1192
 1193
 1194
 1195
 1196
 1197
 1198
 1199
 1200
 1201
 1202
 1203
 1204
 1205
 1206
 1207
 1208
 1209
 1210
 1211
 1212
 1213
 1214
 1215
 1216
 1217
 1218
 1219
 1220
 1221
 1222
 1223
 1224
 1225
 1226
 1227
 1228
 1229
 1230
 1231
 1232
 1233
 1234
 1235
 1236
 1237
 1238
 1239
 1240
 1241
 1242
 1243
 1244
 1245
 1246
 1247
 1248
 1249
 1250
 1251
 1252
 1253
 1254
 1255
 1256
 1257
 1258
 1259
 1260
 1261
 1262
 1263
 1264
 1265
 1266
 1267
 1268
 1269
 1270
 1271
 1272
 1273
 1274
 1275
 1276
 1277
 1278
 1279
 1280
 1281
 1282
 1283
 1284
 1285
 1286
 1287
 1288
 1289
 1290
 1291
 1292
 1293
 1294
 1295
 1296
 1297
 1298
 1299
 1300
 1301
 1302
 1303
 1304
 1305
 1306
 1307
 1308
 1309
 1310
 1311
 1312
 1313
 1314
 1315
 1316
 1317
 1318
 1319
 1320
 1321
 1322
 1323
 1324
 1325
 1326
 1327
 1328
 1329
 1330
 1331
 1332
 1333
 1334
 1335
 1336
 1337
 1338
 1339
 1340
 1341
 1342
 1343
 1344
 1345
 1346
 1347
 1348
 1349
 1350
 1351
 1352
 1353
 1354
 1355
 1356
 1357
 1358
 1359
 1360
 1361
 1362
 1363
 1364
 1365
 1366
 1367
 1368
 1369
 1370
 1371
 1372
 1373
 1374
 1375
 1376
 1377
 1378
 1379
 1380
 1381
 1382
 1383
 1384
 1385
 1386
 1387
 1388
 1389
 1390
 1391
 1392
 1393
 1394
 1395
 1396
 1397
 1398
 1399
 1400
 1401
 1402
 1403
 1404
 1405
 1406
 1407
 1408
 1409
 1410
 1411
 1412
 1413
 1414
 1415
 1416
 1417
 1418
 1419
 1420
 1421
 1422
 1423
 1424
 1425
 1426
 1427
 1428
 1429
 1430
 1431
 1432
 1433
 1434
 1435
 1436
 1437
 1438
 1439
 1440
 1441
 1442
 1443
 1444
 1445
 1446
 1447
 1448
 1449
 1450
 1451
 1452
 1453
 1454
 1455
 1456
 1457
 1458
 1459
 1460
 1461
 1462
 1463
 1464
 1465
 1466
 1467
 1468
 1469
 1470
 1471
 1472
 1473
 1474
 1475
 1476
 1477
 1478
 1479
 1480
 1481
 1482
 1483
 1484
 1485
 1486
 1487
 1488
 1489
 1490
 1491
 1492
 1493
 1494
 1495
 1496
 1497
 1498
 1499
 1500
 1501
 1502
 1503
 1504
 1505
 1506
 1507
 1508
 1509
 1510
 1511
 1512
 1513
 1514
 1515
 1516
 1517
 1518
 1519
 1520
 1521
 1522
 1523
 1524
 1525
 1526
 1527
 1528
 1529
 1530
 1531
 1532
 1533
 1534
 1535
 1536
 1537
 1538
 1539
 1540
 1541
 1542
 1543
 1544
 1545
 1546
 1547
 1548
 1549
 1550
 1551
 1552
 1553
 1554
 1555
 1556
 1557
 1558
 1559
 1560
 1561
 1562
 1563
 1564
 1565
 1566
 1567
 1568
 1569
 1570
 1571
 1572
 1573
 1574
 1575
 1576
 1577
 1578
 1579
 1580
 1581
 1582
 1583
 1584
 1585
 1586
 1587
 1588
 1589
 1590
 1591
 1592
 1593
 1594
 1595
 1596
 1597
 1598
 1599
 1600
 1601
 1602
 1603
 1604
 1605
 1606
 1607
 1608
 1609
 1610
 1611
 1612
 1613
 1614
 1615
 1616
 1617
 1618
 1619
 1620
 1621
 1622
 1623
 1624
 1625
 1626
 1627
 1628
 1629
 1630
 1631
 1632
 1633
 1634
 1635
 1636
 1637
 1638
 1639
 1640
 1641
 1642
 1643
 1644
 1645
 1646
 1647
 1648
 1649
 1650
 1651
 1652
 1653
 1654
 1655
 1656
 1657
 1658
 1659
 1660
 1661
 1662
 1663
 1664
 1665
 1666
 1667
 1668
 1669
 1670
 1671
 1672
 1673
 1674
 1675
 1676
 1677
 1678
 1679
 1680
 1681
 1682
 1683
 1684
 1685
 1686
 1687
 1688
 1689
 1690
 1691
 1692
 1693
 1694
 1695
 1696
 1697
 1698
 1699
 1700
 1701
 1702
 1703
 1704
 1705
 1706
 1707
 1708
 1709
 1710
 1711
 1712
 1713
 1714
 1715
 1716
 1717
 1718
 1719
 1720
 1721
 1722
 1723
 1724
 1725
 1726
 1727
 1728
 1729
 1730
 1731
 1732
 1733
 1734
 1735
 1736
 1737
 1738
 1739
 1740
 1741
 1742
 1743
 1744
 1745
 1746
 1747
 1748
 1749
 1750
 1751
 1752
 1753
 1754
 1755
 1756
 1757
 1758
 1759
 1760
 1761
 1762
 1763
 1764
 1765
 1766
 1767
 1768
 1769
 1770
 1771
 1772
 1773
 1774
 1775
 1776
 1777
 1778
 1779
 1780
 1781
 1782
 1783
 1784
 1785
 1786
 1787
 1788
 1789
 1790
 1791
 1792
 1793
 1794
 1795
 1796
 1797
 1798
 1799
 1800
 1801
 1802
 1803
 1804
 1805
 1806
 1807
 1808
 1809
 1810
 1811
 1812
 1813
 1814
 1815
 1816
 1817
 1818
 1819
 1820
 1821
 1822
 1823
 1824
 1825
 1826
 1827
 1828
 1829
 1830
 1831
 1832
 1833
 1834
 1835
 1836
 1837
 1838
 1839
 1840
 1841
 1842
 1843
 1844
 1845
 1846
 1847
 1848
 1849
 1850
 1851
 1852
 1853
 1854
 1855
 1856
 1857
 1858
 1859
 1860
 1861
 1862
 1863
 1864
 1865
 1866
 1867
 1868
 1869
 1870
 1871
 1872
 1873
 1874
 1875
 1876
 1877
 1878
 1879
 1880
 1881
 1882
 1883
 1884
 1885
 1886
 1887
 1888
 1889
 1890
 1891
 1892
 1893
 1894
 1895
 1896
 1897
 1898
 1899
 1900
 1901
 1902
 1903
 1904
 1905
 1906
 1907
 1908
 1909
 1910
 1911
 1912
 1913
 1914
 1915
 1916
 1917
 1918
 1919
 1920
 1921
 1922
 1923
 1924
 1925
 1926
 1927
 1928
 1929
 1930
 1931
 1932
 1933
 1934
 1935
 1936
 1937
 1938
 1939
 1940
 1941
 1942
 1943
 1944
 1945
 1946
 1947
 1948
 1949
 1950
 1951
 1952
 1953
 1954
 1955
 1956
 1957
 1958
 1959
 1960
 1961
 1962
 1963
 1964
 1965
 1966
 1967
 1968
 1969
 1970
 1971
 1972
 1973
 1974
 1975
 1976
 1977
 1978
 1979
 1980
 1981
 1982
 1983
 1984
 1985
 1986
 1987
 1988
 1989
 1990
 1991
 1992
 1993
 1994
 1995
 1996
 1997
 1998
 1999
 2000
 2001
 2002
 2003
 2004
 2005
 2006
 2007
 2008
 2009
 2010
 2011
 2012
 2013
 2014
 2015
 2016
 2017
 2018
 2019
 2020
 2021
 2022
 2023
 2024
 2025
 2026
 2027
 2028
 2029
 2030
 2031
 2032
 2033
 2034
 2035
 2036
 20

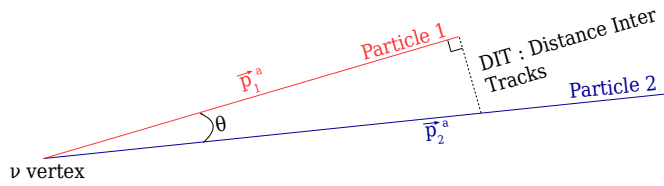


Figure 29: Definition of the distance inter tracks.

618 6.1.2 Performances

619 The particle-only reconstruction efficiencies and the reconstruction threshold in momenta
 620 are shown in Table 7. This threshold is defined as the maximal momentum for which the
 621 reconstruction efficiency is smaller than 30%. The thresholds in muon and pion momenta
 622 are 150 MeV/c. Most of the muons are above this threshold (see Figure 28) which leads
 623 to a 79% reconstruction efficiency.

	μ	π	p
Reconstruction Efficiency	79%	52%	26%
Momentum threshold	150 MeV/c	150 MeV/c	550 MeV/c

Table 7: Reconstruction efficiency and momentum threshold for muons, pions and protons. The threshold is defined as the maximal momentum for which particles have a reconstruction efficiency smaller than 30%.

624 The lower pion and proton efficiencies (respectively 52% and 26%) are due to lower
 625 efficiencies for similar momenta than muons, coming from strong interactions as shown
 626 on Figures 30. Efficiencies of each particle type tend to decrease in the backward region
 627 due to particle lower momenta. However, for a fixed momentum value, the reconstruc-
 628 tion efficiency is almost uniform which confirms the ability of the WAGASCI detector to
 629 reconstruct high angle tracks.

630 The reconstruction is thereafter tested on neutrino events. Table 8 summarizes the
 631 number of reconstructed events and efficiencies for each interaction type. As expected
 632 from the high muon reconstruction efficiency, the charged current interactions have recon-
 633 struction efficiencies $\geq 85\%$.

634 The reconstruction efficiencies as a function of the neutrino energy and muon kinematics
 635 are respectively shown on Figure 31 and 32.

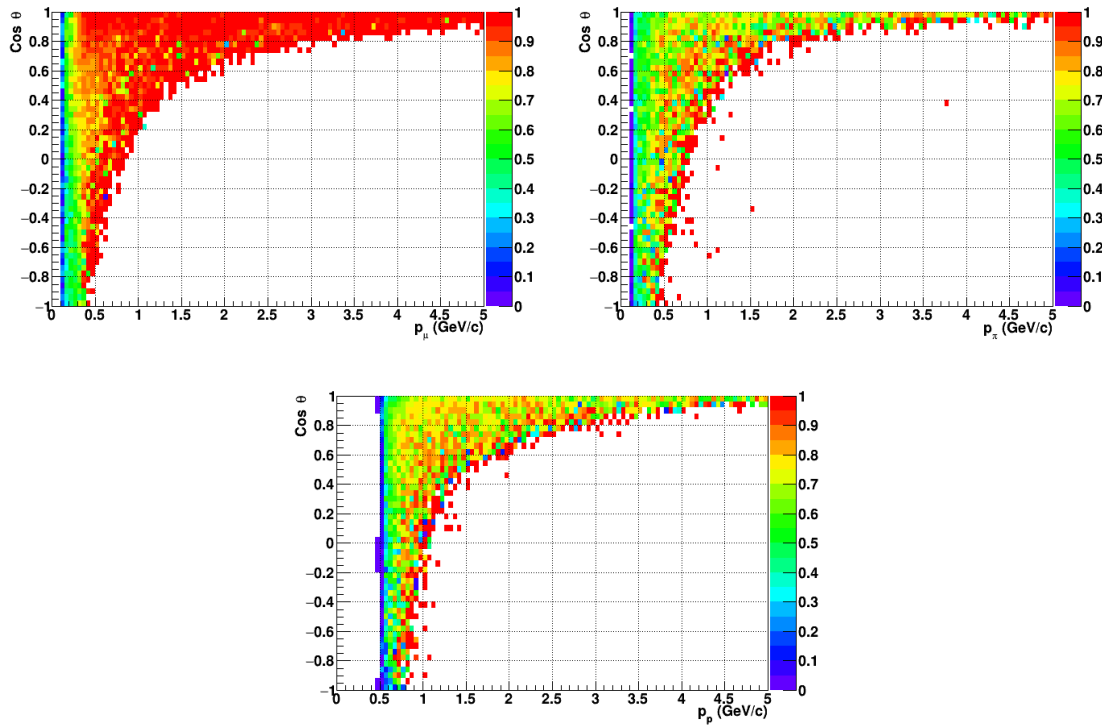


Figure 30: Reconstruction efficiency of muons (left), charged pions (right) and protons (bottom) in the WAGASCI water-module as a function of the particles momenta and angles.

	CC0 π	CC1 π	CCOthers	NC	All
Reconstruction efficiency	85%	87%	91%	22%	68%

Table 8: Number of true interactions reconstructed. The purity and reconstruction efficiency of each true interaction is also shown.

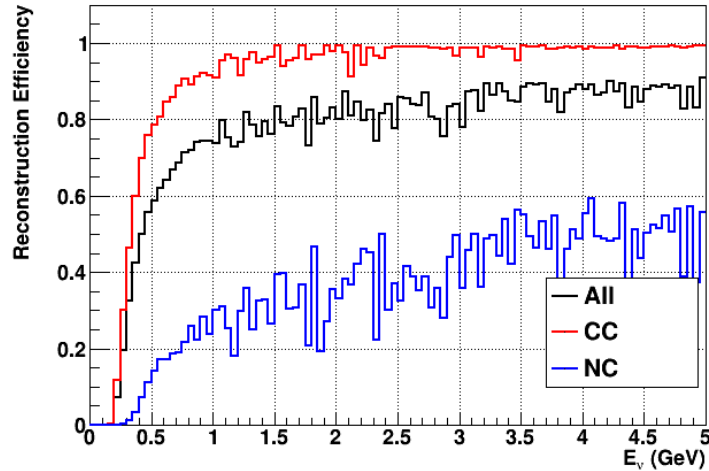


Figure 31: Reconstruction efficiency of all neutrino (black), CC (red) and NC (blue) interactions in the WAGASCI water-module as a function of the neutrino energy.

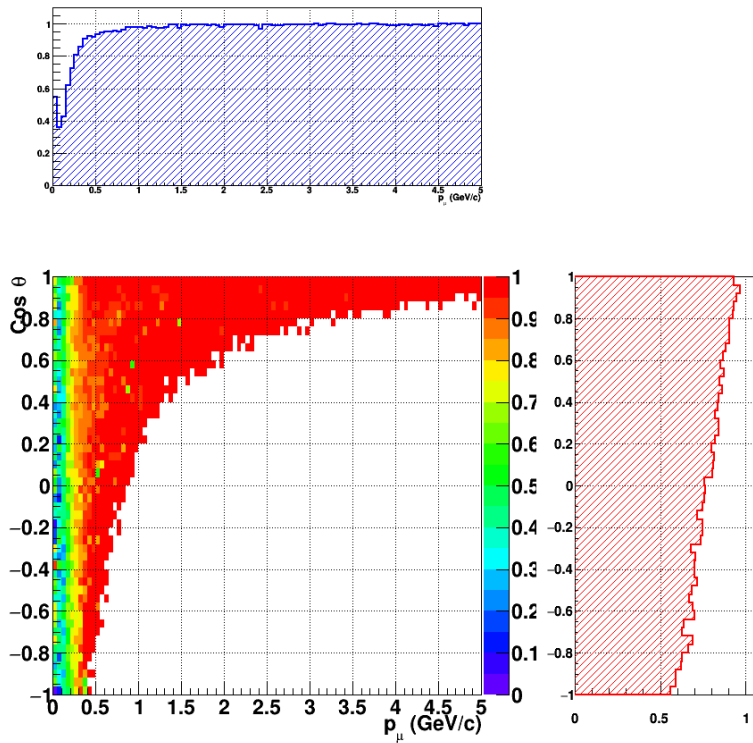


Figure 32: Reconstruction efficiency of CC interactions in the WAGASCI water-module as a function of the muon kinematic variables (momentum and angle).

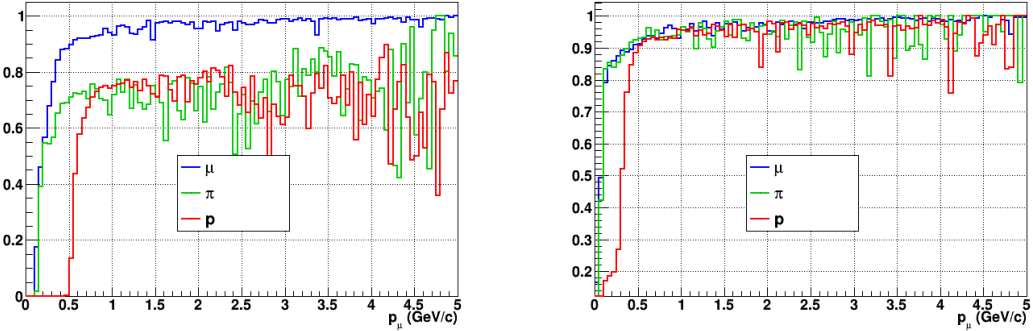


Figure 33: Reconstruction efficiency for muons, pions and protons in the water-in (left) and water-out (right) modules.

636 Note that a Particle Identification Algorithm has been also developed. It is based on
 637 the charge deposition of the particles in the scintillator, of the detection of a decay-electron.
 638 However, this information highly depends on the number of scintillator hit by a particle,
 639 which creates an important difference between a real WAGASCI module and the one used
 640 for the ND280-upgrade simulation. For this reason, the corresponding results will not be
 641 detailed here, but can be found in [?].

642 6.2 Background subtraction: the water-out module

643 In the nominal configuration, 20% of the neutrino interactions occurs on scintillators
 644 (C_8H_8). This background should be removed in order to measure the neutrino interac-
 645 tion on the same target as Super-K, which suppress the differences in cross-section models.
 646 For this purpose, we propose to use a water-out module, where the water is replaced by
 647 air. The detector is therefore fully active and has a 3 mm spatial resolution (scintillator
 648 thickness) which create an ideal detector to reconstruct and identify hadrons, and study
 649 np-nh interactions. The counter-part is the difference in particle energy deposition between
 650 the water and this water-out module that will need to be corrected for. In this section,
 651 we present the capabilities of such a module, and the impact it can have on cross-section
 652 measurements for the neutrino community in general and T2K in particular.
 653 The same reconstruction and selection as the water-in module is applied. Figure 33 shows
 654 the comparison between the water-in and the water-out reconstruction efficiencies for muon,
 655 pions and protons. 90% of the muons and 87% of the pions are reconstructed, while 70%
 656 of the protons are even reconstructed. It allows to lower down the proton threshold to
 657 250 MeV/c (see Table 9).

658 As a consequence of tracking even low momenta particle, the reconstruction efficiency
 659 is uniform and almost maximal on the entire $\cos \theta_\mu$ phase space, as shown on Figure 34.

	μ	π	p
Reconstruction Efficiency Momentum threshold	90% 50 MeV/c	87% 50 MeV/c	70% 250 MeV/c

Table 9: Reconstruction efficiency, proportions of μ -like and non μ -like and momentum threshold for muons, pions and protons in the empty module. The threshold is defined as the maximal momentum for which particles have a reconstruction efficiency smaller than 20%.

660 Since the fiducial mass represents 0.25 tons, the total number of events is divided by a
 661 factor of 3 compared to the water-in module. The water-out module offers interesting
 662 possibilities to study np-nh interaction since 70% of the protons are reconstructed. In the
 663 future, a possible separation as a function of the number of proton track will be studied.
 664 Moreover, we are currently pursuing the use of single and double transverse variables (cite
 665 Xianguo) to open new possibilities for separating np-nh from Final State Interactions, or
 666 for isolating the interactions on hydrogen from interactions on carbon in this module.

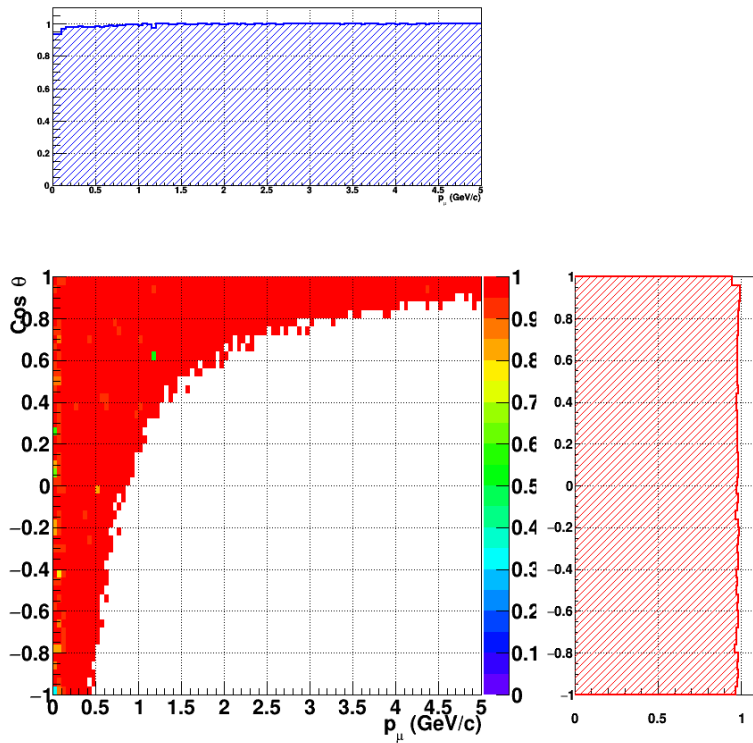


Figure 34: Reconstruction efficiency of CC interactions in the WAGASCI empty module as a function of the muon kinematic variables (momentum and angle).

667 **7 Schedule**

668 We would like to start a physics data taking from T2K beam time after the summer
669 shutdown in 2018. By then, commissioning and tests of the detectors will be completed
670 in J-PARC T59. The experiment can run parasitically with T2K, therefore we request no
671 dedicated beam time nor beam condition as discussed in the following section.

672 Once the approved POT is accumulated, the WAGASCI modules will be removed
673 from the experimental site, but we would like to keep the Baby-MIND and the Side-MRD
674 modules on the B2 floor of the NM pit as common platforms of future neutrino experiments
675 using the T2K neutrino beam.

676 **8 Requests**

677 **8.1 Neutrino beam**

678 The experiment can run parasitically with T2K, therefore we request no dedicated beam
679 time nor beam condition. As data taking periods, we request the ‘nominal’ T2K one-year
680 operation both for the neutrino beam and the antineutrino beam. The T2K has been
681 requesting 0.9×10^{21} POT/year and actually accumulating about 0.7×10^{21} POT/year in
682 recent years. For each year, starting from the Autumn, T2K is running predominantly in
683 the neutrino mode or in the antineutrino mode. Our request is to have one-year neutrino-
684 mode data and another one-year antineutrino mode data assuming that the POT for the
685 fast extraction in each year is more than 0.5×10^{21} POT.

686 **8.2 Equipment request including power line**

687 We request the followings in terms of equipment on the B2 floor:

- 688 • Site for the WAGASCI modules, Side-MRD modules and BabyMIND and their elec-
689 tronics system on the B2 floor of the near detector hall (Fig. 2 and 3).
- 690 • Anchor points (holes) on the B2 floor to secure the WAGASCI modules, Side-MRD
691 module and Baby-MIND, detailed floor plans to be communicated in a separate
692 document.
- 693 • Power line for the magnets in Baby-MIND: 400 V tri-phase 48-to-62 Hz, capable of
694 delivering 12 kW. We have a wish for the magnet power line to be installed and
695 available to us by beginning of March 2018.
- 696 • Electricity for electronics and water circulation system, 3 kW, standard Japanese
697 electrical sockets.

- 698 1. Online PCs: 2.1 kW

699 2. Electronics: 0.7 kW

700 3. Water sensors: 1 kW

- 701 • Air conditioner for cooling heat generation at Baby-MIND magnets, online PCs and
702 electeronics
- 703 • Beam timing signal and spill information
- 704 • Network connection

705 The infrastructure for much of the above exists already. Exceptions are the power line
706 for the magnet and the electronics and holes in the B2 floor to anchor the detector support
707 structures.

708 References

- 709 [1] K. Abe et al. Measurement of the muon neutrino inclusive charged-current cross
710 section in the energy range of 13 GeV with the T2K INGRID detector. *Phys. Rev.*,
711 D93(7):072002, 2016.
- 712 [2] M. Antonova et al. Baby MIND Experiment Construction Status. In *Prospects in*
713 *Neutrino Physics (NuPhys2016) London, London, United Kingdom, December 12-14,*
714 2016, 2017.
- 715 [3] K. Nitta et al. The k2k scibar detector. *Nucl. Instrum. Meth. A*, 535:147, 2004.
- 716 [4] K. Abe et al. (T2K Collaboration). Measurement of the inclusive ν_μ charged current
717 cross section on iron and hydrocarbon in the t2k on-axis neutrino beam. *Phys. Rev.*
718 D, 90:052010, 2014.
- 719 [5] F. Magniette F. Gastaldi, R. Cornat and V. Boudry. A scalable gigabit data acquisition
720 system for calorimeters for linear collider. *proceedings of TIPP2014*, page PoS 193,
721 2014.
- 722 [6] J. Fleury, S. Callier, C. de La Taille, N. Seguin, D. Thienpont, F. Dulucq, S. Ahmad,
723 and G. Martin. Petiroc and Citiroc: front-end ASICs for SiPM read-out and ToF
724 applications. *JINST*, 9:C01049, 2014.
- 725 [7] M. B. Barbaro J. A. Caballero T. W. Donnelly G. D. Megias, J. E. Amaro. Inclusive
726 electron scattering within the susav2 meson-exchange current approach. *Phys. Rev.*
727 D, 94:013012, 2016.
- 728 [8] M. Valverde J. Nieves, J. E. Amaro. Inclusive quasi-elastic neutrino reactions. *Phys.*
729 *Rev. C*, 70:055503, 2004.

- 730 [9] Yu. G. Kudenko, L. S. Littenberg, V. A. Mayatsky, O. V. Mineev, and N. V. Ershov.
731 Extruded plastic counters with WLS fiber readout. *Nucl. Instrum. Meth.*, A469:340–
732 346, 2001.
- 733 [10] O. Mineev, Yu. Kudenko, Yu. Musienko, I. Polyansky, and N. Yershov. Scintillator
734 detectors with long WLS fibers and multi-pixel photodiodes. *JINST*, 6:P12004, 2011.
- 735 [11] Etam Noah et al. Readout scheme for the Baby-MIND detector. *PoS*, Photo-
736 toDet2015:031, 2016.
- 737 [12] Omega. Spiroc 2 user guide. 2009.